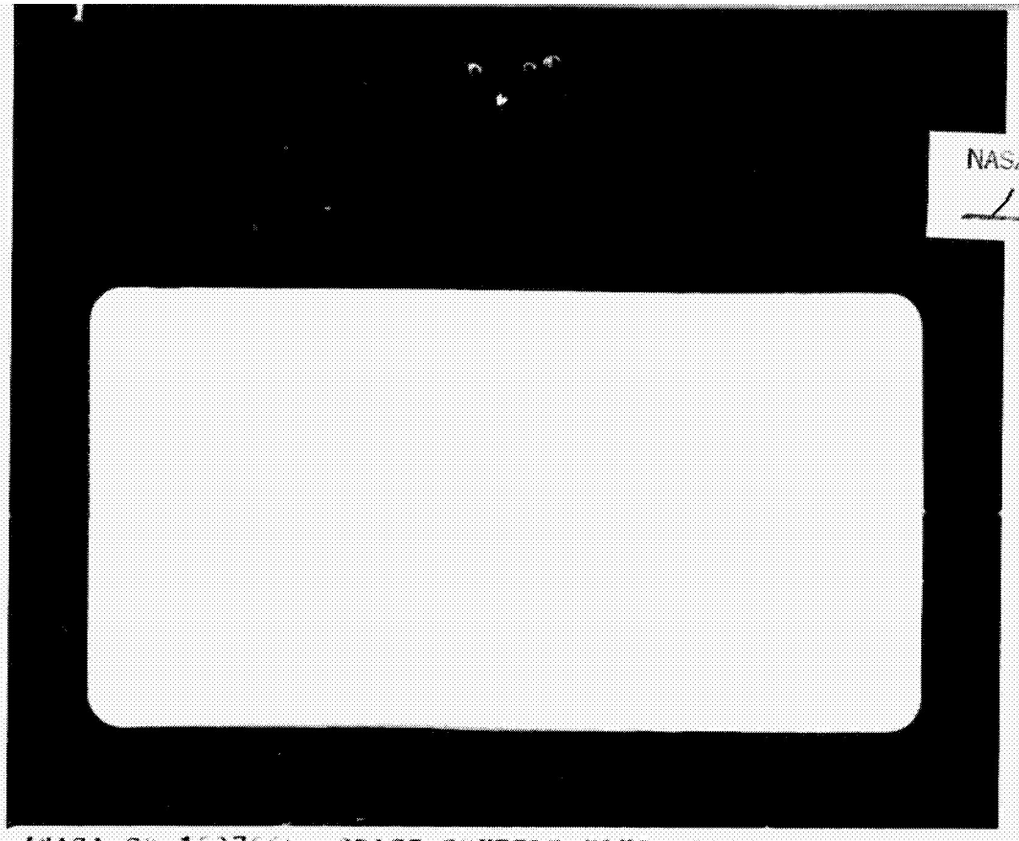

(NASA-CR-160766) SPACE SHUTTLE NAVIGATION ANALYSIS. VOLUME 2: BASELINE SYSTEM NAVIGATION Final Report (Analytic Sciences Corp.) 99 p HC A05/MF A01 CSCL 22A

N80-31441

Unclas
G3/16 28525

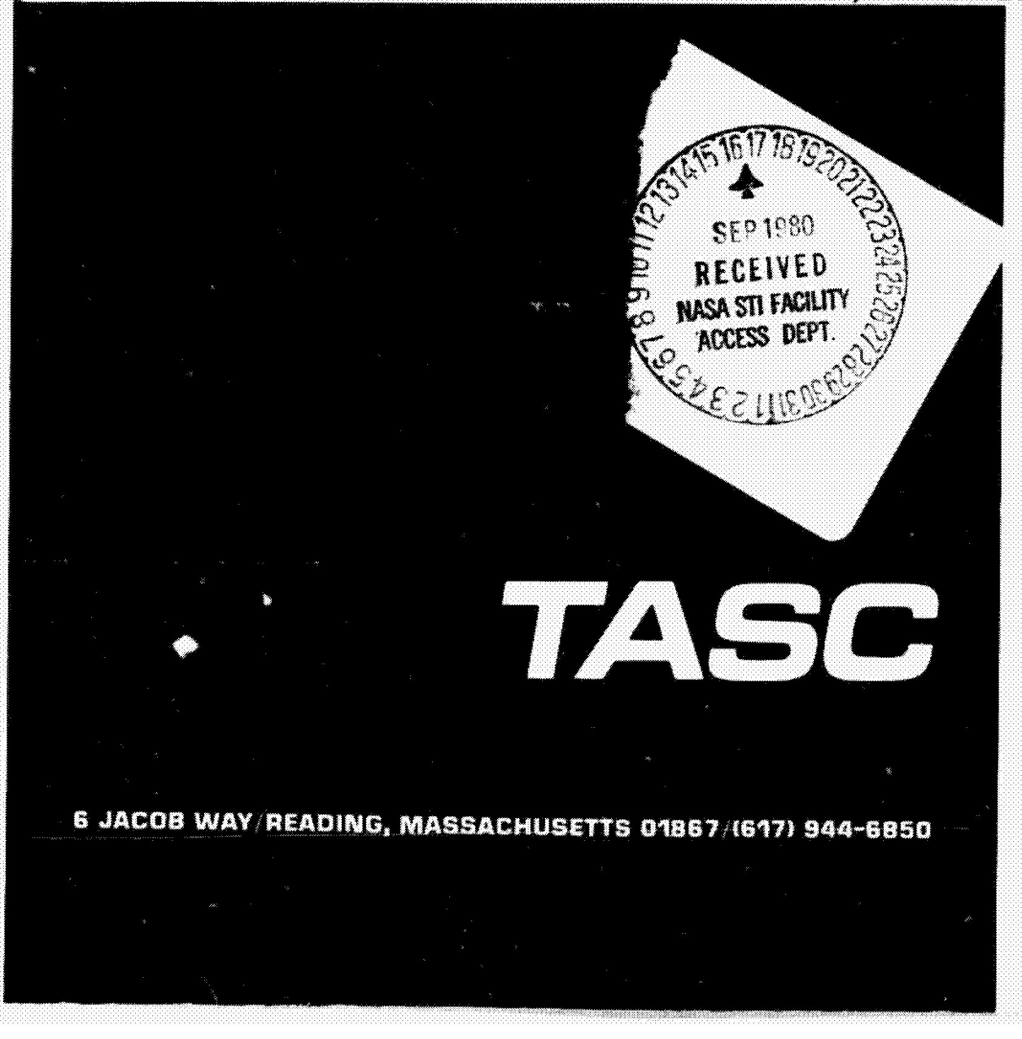

TR-1001-1-1

SPACE SHUTTLE NAVIGATION ANALYSIS
VOLUME II
BASELINE SYSTEM NAVIGATION

30 May 1980

Prepared under

Contract No. NAS9-15151

for

NATIONAL AERONAUTICS AND SPACE ADMINISTRATION
Johnson Space Center
Houston, Texas 77058

Prepared by

Harold L. Jones
Gerd Lüders
Gary A. Matchett
Robert G. Rains

Approved by

E. Wayne Vinje

THE ANALYTIC SCIENCES CORPORATION
Six Jacob Way
Reading, Massachusetts 01867

FOREWORD

The work for this report was performed under contract number Nas 9-15151. The authors acknowledge the guidance and assistance of the Contract Technical Monitors, Messrs. R.T. Savely and E.R. Schiesser of the Math Physics Branch of the Mission Planning and Analysis Division of NASA/JSC. Assistance and co-operation were also received from Messrs. H.G. DeVezin and T.J. Blucker.

ABSTRACT

This report presents the results of several analytical studies related to Space Shuttle Navigation. It is divided into two Volumes, the first dealing with studies related to the addition of NAVSTAR Global Positioning System user equipment to the Shuttle avionics suite, and the second dealing with studies of the baseline avionics suite without GPS. The GPS studies center about navigation accuracy covariance analyses for both developmental and operational phases of GPS as well as for various Orbiter mission phases. The baseline navigation system studies include a covariance analysis of the Inertial Measurement Unit calibration and alignment procedures, postflight IMU error recovery for the Approach and Landing Phases, on-orbit calibration of IMU instrument biases, and a covariance analysis of entry and prelaunch navigation system performance.

TABLE OF CONTENTS

		Page No.
Foreword		ii
Abstract		iii
List of Figures		vi
List of Tables		vii
1.	INTRODUCTION	1-1
	1.1 Shuttle Baseline Navigation Suite	1-1
	1.2 Baseline Navigation Studies	1-1
2.	IMU CALIBRATION AND ALIGNMENT COVARIANCE ANALYSIS	2-1
	2.1 Calibration and Alignment Overview	2-2
	2.2 Covariance Analysis Program Description	2-5
	2.2.1 Program Overview	2-5
	2.2.2 State and Covariance Equations	2-6
	2.3 Truth Model Description	2-9
	2.3.1 States and Error Sources	2-9
	2.3.2 Truth Model Data Base	2-11
	2.3.3 Reliability of IMU Error Model and Data Base	2-21
	2.4 OFT Calibration and Alignment Performance	2-22
	2.4.1 Hangar Calibration Performance	2-23
	2.4.2 Preflight Calibration and Alignment Performance	2-29
	2.4.3 Effect of Accelerometer Scale Factor Attitude Sensitivity	2-36
	2.4.4 Needs for IMU Error Model Improvement	2-38
	2.5 Chapter Summary and Conclusions	2-41
	2.5.1 Summary of Findings	2-41
	2.5.2 Recommendations	2-44
3.	POSTFLIGHT IMU ERROR RECOVERY FOR APPROACH AND LANDING MISSION PHASES	3-1
	3.1 Mission Scenario and System Error Models	3-2
	3.2 Assessment of Potential Error Recovery Performance	3-6
4.	ON ORBIT CALIBRATION OF SHUTTLE IMU ACCELEROMETER AND GYROSCOPE BIASES	
	4.1 Introduction and Summary	4-1
	4.2 Accelerometer Calibration	4-3
	4.3 Gyro Calibration	4-7

TABLE OF CONTENTS (Cont.)

		Page No.
5.	ENTRY AND PRELAND NAVIGATION PERFORMANCE	5-1
	5.1 Revised Navigation Scenario	5-1
	5.2 Navigation System Performance	5-6
6.	SUMMARY AND CONCLUSIONS	6-1
	6.1 IMU Calibration and Alignment Covariance Analysis	6-1
	6.2 Postflight IMU Error Recovery for Approach and Landing Mission Phases	6-2
	6.3 On Orbit Calibration of Shuttle IMU Acclerometer and Gyroscope Biases	6-3
	6.4 Entry and Preland Navigation Performance	6-4
REFERENCES		R-1

LIST OF FIGURES

Figure No.		Page No.
1.1-1	Baseline Navigation Studies Overview	
2.1-1	Calibration and Alignment Schedule	2-4
2.2-1	Structure of Covariance Simulation for Performance Analysis	2-5
2.3-1	Error in a ΔV Pulse Count Due to Quantization	2-19
3.1-1	Ground Track for Sample ALT Trajectory	3-3
3.2-1	Filtered IMU Misalignments for Simulated ALT Mission	3-7
5.1-1	Schedule for Entry, Preland, and Landing Phase Navigation Filter States	5-3

LIST OF TABLES

Table No.		Page No.
2.1-1	Errors Considered During the Cal/Align Phase	2-4
2.2-1	System and Covariance Error Equation Summary	2-7
2.3-1	IMU Truth Model States and Error Sources	2-10
2.3-2	IMU Truth Model Data Base for Calibrated Errors	2-12
2.3-3	IMU Truth Model Data Base for Noncalibrated Errors	2-13
2.3-4	IMU Truth Model Data Base for Heading Sensitive Gyro and Attitude Sensitive Accelerometer Errors	2-14
2.4-1	Hangar Calibration Error Budget	2-24
2.4-2	Preflight Calibration Error Budget	2-30
2.4-3	Preflight Fine Alignment Error Budget	2-31
2.4-4	Detailed Error Budget for Error Group 21 in Hangar Cal A	2-37
2.4-5	Error Amplification Factors for Error Group 21 In Hangar Cal A	2-39
2.4-6	Error Amplification Factors for Error Group 21 In Hangar Cal A	2-40
3.1-1	Time Line for Sample ALT Trajectory	3-3
3.1-2	Assumed Instrumentation Error Model For ALT	3-4
3.1-3	Data Base for IMU-Related Error Sources	3-5
3.2-1	Standard Deviations of Filtered IMU Errors For Sample ALT Mission	3-6
4.2-1	Summary of On-Orbit Accelerometer Bias Calibration Errors	4-7
4.3-1	Extreme Cases For Division of Gyro Errors	4-11

LIST OF TABLES (Cont.)

Table No.		Page No.
5.1-1	Key Events For OFT-1 Mission	5-2
5.1-2	Initial Condition Errors For Revised Filter	5-3
5.1-3	Filter State and Measurement Error Statistics For Entry and Preland Navigation Filter	5-5
5.1-4	Filter-Indicated Performance	5-5
5.2-1	Estimated Performance for Revised Navigation Filter	5-7
5.2-2	Revised Partial Error Budget for The Entry Navigation Phase	5-9
5.2-3	Revised Partial Error Budget At 20,000 Ft.	5-11

1. INTRODUCTION

This is Volume II of a two volume final report on Space Shuttle Navigation Analyses. Volume I is concerned with the addition of GPS user equipment to the Shuttle avionics suite, while this volume treats several topics related to the baseline navigation system for the Orbiter. An introduction to the entire report, relating the current studies to earlier work, is to be found in Volume I. The remainder of this introduction, extracted from that in Volume I, refers only to the work reported here.

1.1 SHUTTLE BASELINE NAVIGATION SUITE

Figure 1.1-1 illustrates the various mission phases of a Space Shuttle flight and helps tie together the various studies of the baseline navigation system reported on in this volume. The elements of the baseline navigation system include Inertial Measurement Units (IMU's) with their inertial sensors, barometric altimeters, TACANS, and a Microwave Landing System (MLS). The MLS is not addressed in the present work; it has been studied in prior work. The other elements of the baseline navigation system are all involved in the studies of this volume.

1.2 SHUTTLE BASELINE NAVIGATION SUITE

There are four areas in which performance of the baseline shuttle navigation system was addressed in this study. These areas

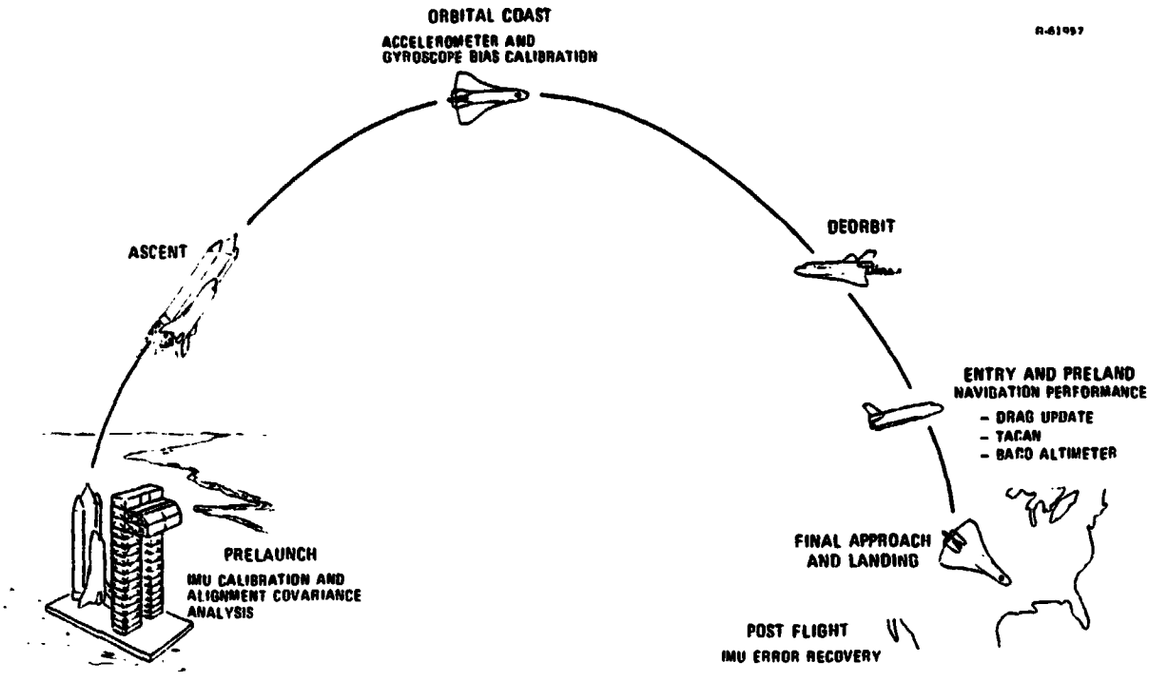

Figure 1.1-1 Baseline Navigation Studies Overview

are related in that they all focus on the performance characteristics of the Orbiter Inertial Measurement Units (IMU's). Three of them involve calibration of the IMU, while the fourth centers on navigation performance.

Preflight calibration and alignment of the IMU's has been studied in prior contracts (Ref. 1), but this report provides the first covariance analysis of the current Orbital Flight Test (OFT) cal/align procedure (covariance analysis results for two prior versions of the OFT cal/align procedure were also generated under this contract -- see Refs. 4 and 5). The previous efforts utilized monte carlo techniques to generate an overall performance projection for the Approach and Landing Tests (ALT), and to identify potential risk areas. The current effort, reported in Chapter 2, uses covariance

techniques to generate overall performance projections, to develop a detailed error budget for the OFT missions, and to identify the major error mechanisms that limit calibration and alignment performance.

ALT provided NASA's first opportunity to evaluate both the navigation performance achievable with the IMU and the true calibration and alignment uncertainties in a flight environment. The study of postflight IMU error recovery reported in Chapter 3 provides a preliminary assessment of the potential accuracy of recovering IMU errors from ALT. The performance specification for the Shuttle IMUs requires that they maintain their prelaunch calibration acucracy for a period of approximately 15 hrs. After lengthy periods on-orbit, the IMU gyros and accelerometers will need recalibration of their observable characteristics (primarily biases) in the weightless environment. In Chapter 4, the best method for performing such a calibration is addressed, and procedures, timings, and analytical techniques are recommended based on laboratory models of the instruments.

In Chapter 5, an assessment of navigation performance during entry but prior to the landing phase is provided. This work is a follow-on to work completed under the previous contract (Ref. 4), but is based on more recent, optimistic assumptions of initial errors and sensor performance, and a revised measurement schedule for the baro altimeter. A candidate, baseline navigation filter is examined in detail.

Chapter 6 is a summary chapter, highlighting the conclusions from all of these baseline navigation system studies.

2. IMU CALIBRATION AND ALIGNMENT COVARIANCE ANALYSIS

The performance analysis for the Space Shuttle Inertial Measurement Unit (IMU) calibration and alignment software has been conducted in two phases. The first phase, completed under a previous contract period (Ref. 1), used monte carlo techniques to generate an overall performance projection for the Approach and Landing Test (ALT) calibration and alignment algorithm (Ref. 2) and to identify potential risk areas. The second phase uses covariance analysis techniques to develop a detailed error budget for the Orbital Flight Test (OFT) algorithm (Ref. 3) and to identify the major error mechanisms which limit calibration and alignment performance. For those error parameters for which the OFT algorithm cannot provide the required calibration accuracy, the results of this phase provide a clear indication as to the algorithm modifications which should be made in order to achieve the desired performance.

An error budget showing the contribution of all error sources to calibration and alignment performance for an earlier version of the cal/align algorithm was presented in Refs 4 and 5. That error budget was applicable to the OFT algorithm defined by Ref. 3, dated December 1976. The cal/align error analysis discussed in this report incorporates all changes made to the OFT algorithm through December of 1978 which may affect cal/align performance. The most important of these changes are:

- New 13-position Hangar Cal A and 7-position Preflight Cal A sequences designed to avoid the effects of the transients induced when switching accelerometers between high and low gain (Ref. 6)

- New Hangar Cal A and Preflight Cal A calibration equations to accommodate the 13-position and 7-position sequences (Ref. 6)
- Modified Hangar Cal A calibration equations for the high gain accelerometer asymmetry errors (Ref. 7)
- Changes to the cal/align sequences for Hangar Coarse Alignment, Preflight Coarse Alignment, and Gyrocompassing
- Incorporation of the accelerometers' double dead band characteristics and its software "fix." An evaluation of the impact of LSF filter estimation accuracy of this effect was reported in Ref. 8
- An update of the IMU error model data base based upon inputs from Singer-Kearfott Division (SKD) and Rockwell International (RI) (Ref. 13-19, and 30)

An overview of the calibration and alignment mechanization for OFT is presented in Section 2.1. Section 2.2 contains a general description of the mathematical structure used in the covariance simulations, and Section 2.3 summarizes the truth model states and error sources used in the covariance analysis. An error budget showing the contribution of all error sources to calibration and alignment performance, as well as a discussion of the results obtained, is presented in Section 2.4.

2.1 CALIBRATION AND ALIGNMENT OVERVIEW

The calibration and alignment of the Space Shuttle IMUs consists of two parts: Hangar Calibration, and Preflight Calibration and Alignment. Hanger Calibration will be performed

in a low-vibration environment† within 5* to 14* days prior to launch, and will have a total duration of 9.6* hr. Preflight Calibration and Alignment will be initiated at the launch pad within 3* to 15* hr before launch, and will have a total duration of 3.1* hr. The calibration and alignment schedule during both the hangar and the preflight mission phases is illustrated in Fig. 2.1-1.

The cal/align mechanization consists of steering the platform to a series of discrete positions at which torquing rates are applied to compensate for earth rate, and in some cases "excess" rates are applied to torque the platform through a prescribed trajectory relative to a local vertical (North, West, Up) coordinate system. At each of these positions, the accelerometer outputs and/or the resolver outputs are sampled and a least squares fit (LSF) filter is used to estimate the acceleration along the up axis, the platform tilts and tilt rates about the north and west axes, and/or the platform attitude and attitude rate. Once all data (vertical accelerations, tilts, etc. for each discrete position) have been collected, a number of IMU errors are estimated and the corresponding error compensation parameters are updated. Between discrete positions, the platform is slewed at a high rate and no data is collected during this motion.

The cal/align mechanization is comprised of six different sequences. Each of these consists of several positions and is used for the calibration, alignment, or verifciation of several IMU errors as outlined in Table 2.1-1.

---

†For the OFT mission, Hangar Calibration is performed on the launch pad, this is reflected in the results reported here.

*These times are approximate and subject to modification.

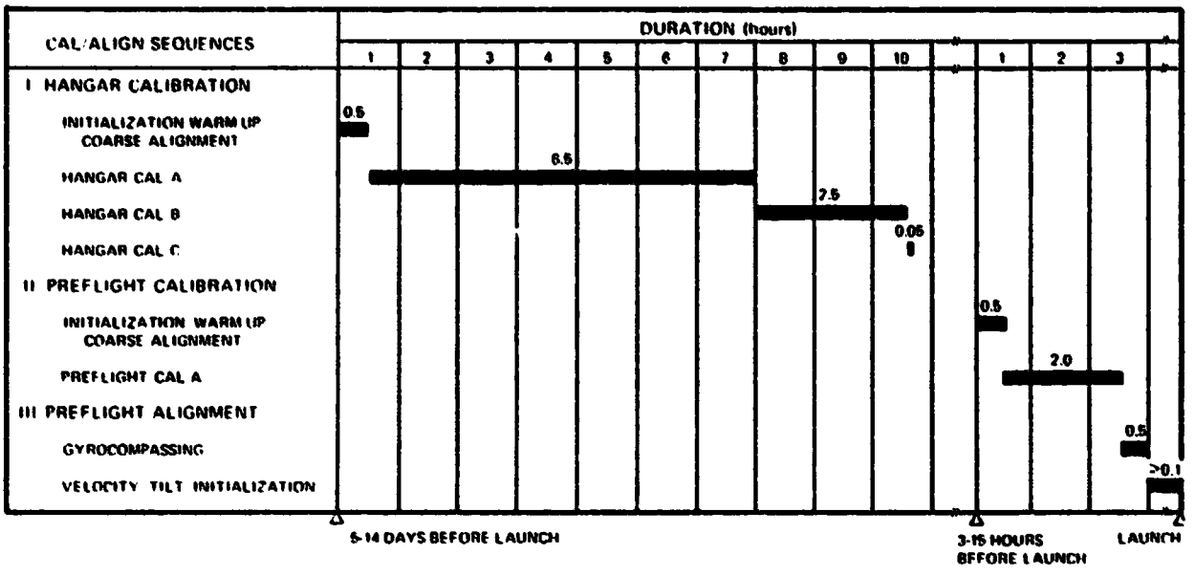

Figure 2.1-1 Calibration and Alignment Schedule

TABLE 2.1-1

ERRORS CONSIDERED DURING THE CAL/ALIGN PHASE

T-0010

IMU Errors		Hangar			Preflight		
Name	No. of Errors	Cal A	Cal B	Cal C	Cal A	Gyro-compass	VTI
Accel. Bias High Gain	3	1			1		
Accel. Scale Factor High Gain	3	1			1		
Accel Bias Low Gain	3	1			1		
Accel. Scale Factor Low Gain	3	1			1		
Gyro Bias Drift Rate	3	1			1		
Gyro Mass Unbalance	5	1			2		
Accel. Scale Factor Asymmetry	3	1					
Accel. Nonorthogonality	3	1					
Gyro Torquer Scale Factor	3	1					
Gyro Misalignment	6	1					
Resolver Offset	3		1				
Gimbal Nonorthogonality	1		1				
Accel. and Gyro to Platform Misalignment	2		1				
Relative Cluster Misalignment	2			3		4	
Level Misalignment	2					5	5
Azimuth Misalignment	1					5	

Key 1 - Estimate and calibrate
2 - Estimate and calibrate the spin and output axis terms
3 - Estimate and store
4 - Estimate and check for reasonableness
5 - Estimate and align

2.2 COVARIANCE ANALYSIS PROGRAM DESCRIPTION

2.2.1 Program Overview

The structure of the covariance analysis program is the same as that of the OFT IMU software. The program is organized into seven separate sequences with an executive program which defines the interface between those sequences (Fig. 2.2-1). The input to the Coarse Alignment sequence is a data file which defines the IMU status (values for all error coefficients, gyro torquing rates, etc.), a priori calibration and alignment estimates, and the transformation matrices between the platform coordinate system and the vehicle-, earth- and inertially-fixed coordinate systems. The output of the Coarse Alignment sequence is a new data file updated by the Coarse Alignment estimates. This file is then the input to Hangar Cal A and so on.

The program preserves the correlation between estimation errors in different sequences and has the capability of simulating a complete calibration and alignment procedure

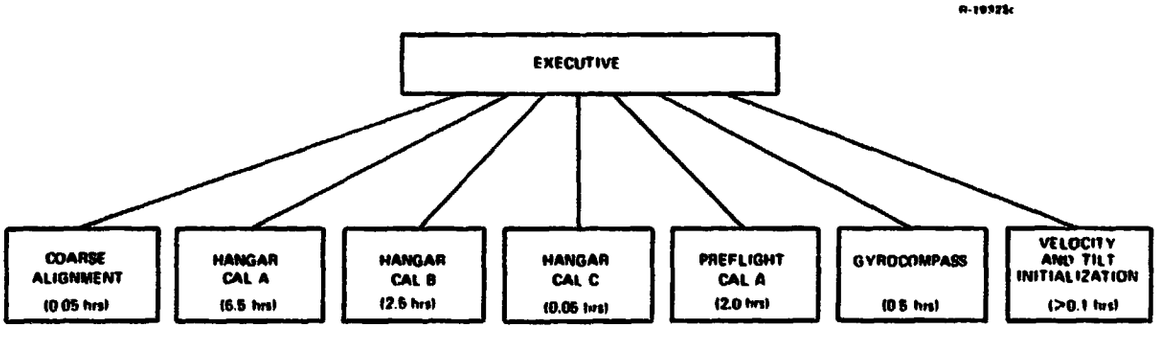

Figure 2.2-1 Structure of Covariance Simulation for Performance Analysis

from beginning to end. Alternatively, the initial condition data for any sequence can be used (and modified if desired) for performing special studies for any other given sequence.

2.2.2 State and Covariance Equations

The LSF filter used in the cal/align software is a recursive filter, i.e., the tilt and tilt rate estimates generated at a particular time are a function only of the current acceleromter outputs and the estimates generated at the previous time. This recursive property permits the estimation procedure to be modeled as a (suboptimal) state estimator for the IMU error parameters based on a linearized model of the system dynamics. Because of the fact that the IMU paramter estimates are updated only at the end of each cal/align sequence, however, it is necessary to introduce temporary storage states into the filter equations. The form of these equations and the approach used in the program to generate the accompanying covariance equations are discussed in this section.

The state and covariance error equations are summarized in Table 2.2-1. Equation 2.2-1, found in the table, models the error propagation for the linearized IMU system. This equation represents the fundamental operational mode of the IMU including its associated software during the Hangar and Preflight phases (the Ground Sequence, Ref. 3). The state vector $\underline{x}$ is composed of three parts:

$\underline{x}_1$ - the least squares fit (LSF) filter states used to estimate the platform accelerations (tilts) and acceleration rates (tilt rates) by measuring the platform velocity outputs, and/or to estimate the platform attitude and attitude rate by measuring the gimbal angles.

TABLE 2.2-1
SYSTEM AND COVARIANCE ERROR EQUATION SUMMARY

T-0046

CAL ALIGN STEP	STATE EQUATION	COVARIANCE EQUATION
ESTIMATE TILTS AND DRIFTS PROPAGATE IMU ERRORS	$\dot{\underline{x}} = F\,\underline{x} + \underline{w}$ (2.2-1)	$\dot{P} = F\,P + P\,F^T + Q$ (2.2-2)
TORQUE OUT TILTS RESET FILTER	$\underline{x}^+ = L\,\underline{x}^-$ (2.2-3)	$P^+ = L\,P^-\,L^T$ (2.2-4)
STORE ESTIMATES RESET FILTER	$\underline{x}^+ = C\,\underline{x}^-$ (2.2-5)	$P^+ = C\,P^-\,C^T$ (2.2-6)
UPDATE IMU PARAMETERS RESET STORAGE STATES	$\underline{x}^+ = D\,\underline{x}^-$ (2.2-7)	$P^+ = D\,P^-\,D^T$ (2.2-8)

Where the vectors are defined by

$$\underline{x}^T = \begin{bmatrix} \underline{x}_1 \\ \underline{x}_2 \\ \underline{x}_3 \end{bmatrix}^T = \begin{bmatrix} \text{LSF Filter States} \\ \text{Storage States} \\ \text{IMU Error States} \end{bmatrix}^T \qquad \underline{w} = \begin{bmatrix} \underline{w}_1 \\ 0 \\ \underline{w}_3 \end{bmatrix} = \begin{bmatrix} \text{Measurement Noise} \\ - \\ \text{Process Noise} \end{bmatrix}$$

and the matrices are given by

IMU DYNAMICS

$$F = \begin{bmatrix} 0 & 0 & KH \\ 0 & 0 & 0 \\ 0 & 0 & F_3 \end{bmatrix}$$

ERROR COVARIANCE

$$P = \begin{bmatrix} P_{11} & P_{12} & P_{13} \\ P_{12} & P_{22} & P_{23} \\ P_{13} & P_{23} & P_{33} \end{bmatrix}$$

NOISE COVARIANCE

$$Q = \begin{bmatrix} R_{11} & 0 & 0 \\ 0 & 0 & 0 \\ 0 & 0 & Q_{33} \end{bmatrix}$$ (2.2-9)

PLATFORM LEVELING

$$L = \begin{bmatrix} 0 & 0 & 0 \\ 0 & I & 0 \\ -L_3 & 0 & I \end{bmatrix}$$

DATA STORAGE

$$C = \begin{bmatrix} 0 & 0 & 0 \\ C_2 & I & C_3 \\ 0 & 0 & I \end{bmatrix}$$

PARAMETER UPDATE

$$D = \begin{bmatrix} 0 & 0 & 0 \\ 0 & D_2 & 0 \\ 0 & -D_3 & I \end{bmatrix}$$ (2.2-10)

$\underline{x}_2$ - the storage states, used to store some of the filter estimates, $\underline{x}_1$, which will be used to update IMU error paramters at a future time.

$\underline{x}_3$ - the system states, including platform velocity errors, misalignments, and all IMU error states being considered in the present cal/align evaluation.

Equation 2.2-1 is driven by white process noise represented by the vector $\underline{w}$. The components of $\underline{w}$ are resolver measurement error $\underline{w}_1$ and the IMU process noise $\underline{w}_3$. There are no errors associated with the transfer of filter states $\underline{x}_1$ into storage states $\underline{x}_2$. The propagation of the statistics associated with the state vector $\underline{x}$ is governed by Eq. 2.2-2. The details about the elements in F_3 and H are given in Appendix B of Ref. 9. Details about the remaining matrices are given in Ref. 10.

At the end of each estimation period some of the filter estimates $\underline{x}_1$ are stored in the temporary memory states $\underline{x}_2$, and, simultaneously, the filter states are reset to zero. This storage and reset is represented by Eqs. 2.2-5 and 2.2-6. Depending on the particular point in the cal/align process, the next step may be one of the following:

- Update one or more of the IMU errors, $\underline{x}_3$, using one or more of the estimates stored in $\underline{x}_2$, and reset the storage states in $\underline{x}_2$, which are not required for future IMU error updates. This step is represented by Eqs. 2.2-7 and 2.2-8
- Rotate the platform about the horizontal axes by an amount equal and opposite to the filter estimates of the platform misalignments from level. This step is represented by Eqs. 2.2-3 and 2.2-4
- Initiate the next estimation of platform tilts and drifts and IMU error propagation, as described above and represented by Eqs. 2.2-1 and 2.2-2.

The cal/align evaluation performed by TASC is based on computation of the covariance Eqs. 2.2-2, 2.2-4, 2.2-6 and 2.2-8. Since the corresponding state Eqs. 2.2-1, 2.2-3, 2.2-5 and 2.2-7 are all linear, it is possible to initialize the matrices P and Q with only those error sources of interest

at a particular time and to obtain, at the end of the run, the sensitivity of the cal/align mechanization to that particular error source or group of errors.

2.3 TRUTH MODEL DESCRIPTION

Generation of an error budget for the cal/align software requires that a "truth model"* describing the real world error sources for the cal/align process be defined. The description must include a complete list of states and error sources, and a data base. The truth model used to evaluate the Space Shuttle IMU cal/align performance is presented in this section. This model incorporates all changes to the baseline OFT algorithm mentioned at the outset of this Chapter.

2.3.1 States and Error Sources

The truth model states and error sources used in evaluating the IMU cal/align mechanization are listed in Table 2.3-1, which divides them into three major categories:

- Category I - Platform misalignments and calibrated IMU error states
- Category II - Noncalibrated IMU error states
- Category III - Random and quantization errors

These three categories contain the error sources which will be used to generate the baseline error budget. The first category corresponds to the platform misalignments

*The "truth model" is a mathematical model of all potentially significant error sources and the way they affect the cal/align performance in the real world.

TABLE 2.3-1
IMU TRUTH MODEL STATES AND ERROR SOURCES

T-0041a

ERROR SOURCE NAME AND GROUP NUMBER	NUMBER OF STATES	NUMBER OF ERROR SOURCES	ERROR MNEMONIC
I. PLATFORM MISALIGNMENTS AND CALIBRATED ERRORS			
1. Platform Misalignment	3	0	
2. Gyro Bias Drift	3	3	DFX,Y,Z
3. Gyro Mass Unbalance	5	5	DIX,Z,DSX,Z,DOZ
4. Gyro Torquer Scale Factor	3	3	KTX,Y,Z
5. Gyro Misalignment	6	6	BXY,XZ,....ZY
6. Accel. Bias -Low Gain	3	3	KOX,Y,Z
7. Accel. Scale Factor -Low Gain	3	3	K1X,Y,Z
8. Accel. Bias -High Gain	3	3	KOHX,Y,Z
9. Accel. Scale Factor -High Gain	3	3	K1HX,Y,Z
10. Accel. Scale Factor Asymmetry	6	6	KSX,Y,Z,KSHX,Y,Z
11. Accel. Nonorthogonality	3	3	DELTYX,ZX,ZY
12. Accel. and Gyro Misalignment	2	2	MXZ,MYZ
13. Resolver Offset, Gimbal Nonorthogonality	4	6	IRO,PO,AZO,DP,a,b
II. NONCALIBRATED IMU ERRORS			
14. Gyro Anisoelasticities	11	11	DI2X,Z,DS2X,Y,Z DISX,Z,DOSX,Z,DIOX,Z
15. Gyro Output Axis Mass Unbalance	2	2	DOX,Y
16. Gyro Heading Sensitive Drift	18	18	HS(X,Y,Z)(OR,P,AZ)
17. Gyro Thermal Transient Drift	3	3	TTX,Y,Z
18. Accel. Nonlinearity - 2^{nd} Order	6	6	K2X,Y,Z,XZ,YZ,ZX
19. Accel. Nonlinearity - 3^{rd} Order	3	3	K3X,Y,Z
20. Accel. Attitude Sensitive Bias	18	18	KOAS(X,Y,Z) (OR,P,AZ)
21. Accel. Attitude Sensitive Scale Factor	18	18	K1AS(X,Y,Z) (OR,P,AZ)
22. Outer Roll Offset and Misalignment	3	3	ORO,AY,AZ
23. Resolver Harmonic	24	24	1^{st},4^{th},8^{th},9^{th}
III. RANDOM AND QUANTIZATION ERRORS			
24. Gyro Randomness and Quantization	3	6	
25. Accel. Randomness and Quantization		6	
26. Resolver Randomness and Quantization		7	
27. Vehicle Motion	7	2	
TOTALS	160	173	

[1]Only three errors are calibrated.

and those IMU error sources which are calibrated during one or more calibration sequences. Category II corresponds to additional IMU error sources which are not estimated or calibrated during either hangar or preflight calibration. Category III contains those states which are driven by random errors, including instrument randomness, quantization effects, and vehicle motions induced by wind gusts.

All error source categories are divided into smaller sets, each of which is associated with a group number. These group numbers are useful in defining the detailed truth model equations in Appendix B of Ref. 9. In addition, each line of the error budget generated in this study will correspond to the contribution from all error sources in one particular group rather than each error taken one at a time. This simplifies the error budget table and places the various error source groups in better perspective.

2.3.2 Truth Model Data Base

Generation of a detailed error budget requires the numerical values for all truth model error sources. Two sets of errors must be specified: the initial calibration error (instrument error minus software compensation term) at the beginning of the hangar calibration phase, and the changes of the instrument errors during the time elapsed between the hangar calibration and the preflight calibration due to the turn-off turn-on errors. This data is summarized in Tables 2.3-2 through 2.3-4; all error terms which were modified from those used by TASC in an earlier cal/align performance evaluation (Refs. 4 and 5) are marked with a "†."

TABLE 2.3-2
IMU TRUTH MODEL DATA BASE FOR CALIBRATED ERRORS

T-3276

ERROR SOURCE NAME AND GROUP NUMBER	UNITS	STANDARD DEVIATION AND SOURCE OF DATA			
		AT BEGINNING OF HANGAR CAL.		TURN-OFF TURN-ON INSTABILITIES	
2. Gyro Bias Drift	arc sec/sec	0.035	Ref. 1	0.035†	Ref. 11
5. Gyro Mass Unbalance					
Input Axis Acceleration	arc sec/sec/g	0.300	Ref. 1	0.025†	Ref. 11
Spin Axis Acceleration	arc sec/sec/g	0.020	Ref. 1	0.025†	Ref. 11
Output Axis Acceleration	arc sec/sec/g	0.025	Ref. 1	0.025†	Ref. 11
4. Gyro Torquer Scale Factor	ppm	400	Ref. 1	100	Ref. 1
5. Gyro Misalignment	arc sec	120	Ref. 1	60†	Ref. 11
6. Accel. Bias - Low Gain:					
X,Y	μg	100	Ref. 1	50	Ref. 11
Z	μg	200	Ref. 1	50	Ref. 11
7. Accel. Scale Factor - Low Gain	ppm	200	Ref. 1	100	Ref. 11
8. Accel. Bias - High Gain:					
X,Y	μg	100	Ref. 1	50	Ref. 11
Z	μg	200	Ref. 1	50	Ref. 11
9. Accel. Scale Factor - High Gain	ppm	200	Ref. 1	100	Ref. 11
10. Accel. Scale Factor Asymmetry:					
High and Low Gain, Correlated*	ppm	200†	Ref. 1	20†	See Text
High and Low Gain, Uncorrelated*	ppm	55†	See Text	0†	See Text
11. Accel. Nonorthogonality	arc sec	60	Ref. 1	21†	Ref. 11
12. Accel. and Gyro Misalignment	arc sec	60	Ref. 1	15†	Ref. 11
13. Resolver Offset	arc sec	200	Ref. 1	20	Ref. 1
Gimbal Nonorthogonality	arc sec	60	Ref. 1	0	Ref. 1

*The high to low gain accelerometer scale factor difference is not calibrated.

†These error terms differ from those given in Ref. 4; they are discussed in the text.

The numerical values described above are required to construct F, P and Q in Eq. 2.2-2. The specified elements of F, P and Q which must be assigned are:

P_{33} - the initial IMU error covariance matrix

ΔP_{33} - the IMU turn-off turn-on instability error covariance matrix

Q_{33} - the process noise covariance matrix

TABLE 2.3-3
IMU TRUTH MODEL DATA BASE FOR NONCALIBRATED ERRORS

T-3277

ERROR SOURCE NAME	UNITS	STANDARD DEVIATION	DATA SOURCE
14. Gyro Anisoelasticity:			
Input-Input Anisoel. Drift	$\widehat{sec}/sec/g^2$	0.005	Ref. 12
Spin-Spin Anisoel. Drift	$\widehat{sec}/sec/g^2$	0.005	Ref. 12
Input-Spin Anisoel. Drift	$\widehat{sec}/sec/g^2$	0.025	Ref. 12
Output-Spin Anisoel. Drift	$\widehat{sec}/sec/g^2$	0.025	Ref. 12
Input-Output Anisoel. Drift	$\widehat{sec}/sec/g^2$	0.005	Ref. 12
15. Gyro Output Axis Mass Unbalance	$\widehat{sec}/sec/g$	0.005	Ref. 12
16. Gyro Heading Sensitive Drift	$\widehat{sec}/sec$	See Table 2.3-4*	See Text
17. Gyro Thermal Transient Drift	$\widehat{sec}/sec$	$0.01\ e^{-t/120}$ (1)+	See Text
18. Accel. Nonlinearity - Second Order		Low Gain / High Gain	
Quadratic	$\mu g/g^2$	15 / 150+	See Text
Product Nonlinearity	$\mu g/g^2$	10 / 100+	See Text
19. Accel. Nonlinearity - Third Order	$\mu g/g^3$	5 / 50+	See Text
20. Accel. Attitude Sensitive Bias	μg	See Table 2.3-4*	See Text
21. Accel. Attitude Sensitive Scale Factor	ppm	See Table 2.3-4*	See Text
22. Outer Roll Offset and Misalignment	$\widehat{sec}$	200	Ref. 1
23. Resolver Harmonic			
1^{st} Harmonic	$\widehat{sec}$	7.6(2)	Ref. 12
8^{th} Harmonic	$\widehat{sec}$	19.0(2)	Ref. 12
9^{th} Harmonic	$\widehat{sec}$	4.2(2)	Ref. 12
16^{th} Harmonic	$\widehat{sec}$	20.0(2)	Ref. 12
24. Gyro Randomness	$\widehat{sec}/sec^{3/2}$	2.89×10^{-5}	See Text
25. Accel. Output Noise	μg	5.0	Ref. 1
Velocity Quantization-Low Gain	ft/sec	See Text	See Text
Velocity Quantization-High Gain	ft/sec	See Text	See Text
26. Resolver Output Noise	$\widehat{sec}$	10.0	See Text
Resolver Quantization	$\widehat{sec}$	5.8	See Text
27. Vehicle Motion		See Text	See Text

(1) t = seconds after completing a cluster repositioning.

(2) Standard deviation of maximum amplitude.

*These error terms differ from those given in Ref. 4; they are discussed in the text.

TABLE 2.3-4

IMU TRUTH MODEL DATA BASE FOR HEADING SENSITIVE GYRO AND ATTITUDE SENSITIVE ACCELEROMETER ERRORS

T-3278

GYRO OR ACCEL. AXIS	GIMBAL	ERROR TERM*	STANDARD DEVIATION OF ERROR COEFFICIENT		
			16. Gyro Drift ($\widehat{sec}$/sec)	20. Accel. Bias (μg)	21. Accel. Scale Factor (ppm)
X	Roll	sin (2φ)	0.004	4.3	13.4
		cos (2φ)	0.004	4.3	13.4
	Pitch	sin (2θ)	0.004	4.3	7.1†
		cos (2θ)	0.004	4.3	7.1†
	Azimuth	sin (2ψ)	0.008	3.7	11.5
		cos (2ψ)	0.008	3.7	11.5
Y	Roll	sin (2φ)	0.004	1.1	3.4
		cos (2φ)	0.004	1.1	3.4
	Pitch	sin (2θ)	0.004	2.2	6.7
		cos (2θ)	0.004	2.2	6.7
	Azimuth	sin (2ψ)	0.008	3.7	11.5
		cos (2ψ)	0.008	3.7	11.5
Z	Roll	sin (2φ)	0.008	2.2	6.7
		cos (2φ)	0.008	2.2	6.7
	Pitch	sin (2θ)	0.008	4.3	7.1†
		cos (2θ)	0.008	4.3	7.1†
	Azimuth	sin (2ψ)	0.006†	3.5	11.0†
		cos (2ψ)	0.006†	3.5	11.0†

*φ, θ, and ψ represent roll, pitch, and azimuth gimbal angle, respectively.

†These error terms differ from those given in Ref. 4; they are discussed in the text.

F_{33} - the IMU truth model error dynamics matrix

R_{11} - the measurement error covariance matrix

Elements of P_{33}, Q_{33}, and F_{33} are normally chosen together to define random processes with desired properties. For instance, a first-order markov process (exponentially correlated random

process) is modeled with a specified rms value, σ_i, and correlation time, τ_i. In this case the relevant truth model matrix elements are:

$$P_{33_{ii}} = \sigma_i^2 \qquad (2.3\text{-}1)$$

$$F_{33_{ii}} = -1/\tau_i \qquad (2.3\text{-}2)$$

$$Q_{33_{ii}} = 2\sigma_i^2/\tau_i \qquad (2.3\text{-}3)$$

A constant error source can be considered a special case of the above with $\tau_i = \infty$ and $F_{33_{ii}} = Q_{33_{ii}} = 0$.

Special characteristics of some of the error groups shown in Tables 2.3-2 through 2.3-4 are discussed below. All error terms whose numerical values were modified from those used by TASC in an earlier cal/align performance evaluation (Refs. 4 and 5) are pointed out; these are marked with a "†" in Tables 2.3-2 through 2.3-4.

Preliminary versions of Tables 2.3-2 through 2.3-4 were reviewed with SKD (Ref. 13). Based on SKD's recommendations, the acclerometer scale factor pitch gimbal sensitivity terms in Tables 2.3-2 through 2.3-3 were reduced; these are discussed under the heading "Groups 16, 20, and 21".

Group 10: Acceleromter Scale Factor Asymmetries (Table 2.3-2) - The model for Group 10 in Ref. 4 assumed uncorrelated low and high gain scale factor asymmetry errors. Since both types of errors were being calibrated, the magni-

tude and degree of correlation of these errors was not important. More recent test data, however, has indicated the following (Ref. 14):

- The high and low gain asymmetry errors are partially correlated
- The difference between high and low gain asymmetry errors is at most 100 ppm (3σ)
- Certain accelerometer errors (including Groups 18 and 19 -- accelerometer nonlinearities) are ten times larger in high gain than in low gain, which can lead to difficulties in calibrating the high gain scale factor asymmetry.

A Software Change Request (Ref. 7) was formulated to remedy the latter problem by using only low gain measurements to calibrate both high and low gain accelerometer asymmetry errors. Accordingly, the new model for Group 10 in Table 2.3-2 exhibits a 200 ppm rms correlated error with a 20 ppm turn-off turn-on instability for the low gain asymmetry error. The high gain asymmetry error equals the low gain error plus an uncorrelated error of 33 ppm (100 ppm, 3σ) with no turn-off turn-on instability. Note that now the uncorrelated part of the high gain asymmetry error is not calibrated. This shortcoming is deemed less serious than the errors that are introduced when attempting to calibrate the high gain asymmetry errors using high gain accelerometer data (Ref. 14).

Turn-off Turn-on Instabilities (Table 2.3-2) - All error terms marked with a "†" were increased in magnitude from those used in Ref. 4. The new values are the long-term stability errors specified in Ref. 8. These changes were recommended by SKD (Ref. 15). The values for error Group 10 are discussed in the foregoing paragraph.

Groups 16, 20, and 21: Heading Sensitive Drift and Attitude Sensitive Bias and Scale Factor (Table 2.3-4) - Each of these IMU error sources is modeled as the sum of three, two-cycle sinusoidal errors, one each for the outer roll, pitch and azimuth gimbal angles. For the baseline error budget presented in Sections 2.4.1 and 2.4.2, the phase of each sinusoid is assumed random, and thus each sinusoid is modeled as the sum of a sine term and a cosine term that are independent and have equal rms magnitudes as listed in Table 2.3-4.

The majority of the error magnitudes shown in Table 2.3-4 were deduced from SKD test data reported in Ref. 16. Based on several discussions with RI and SKD, several errors were modified as follows:

- The rms Z-gyro azimuth heading sensitivities were reduced from 0.025 to 0.006 $\widehat{\text{sec}}$/sec. This change results from an improved heater design. It is based upon test data reported in Ref. 30.
- The Z-accelerometer scale factor and bias azimuth attitude sensitivities were reduced by a factor of 2, to 11.0 ppm and 3.5 μg, respectively. These new values are based on test data reported in Ref. 30. Nevertheless, these errors continue to be significant contributors to cal/align inaccuracies because the 13-position calibration sequence is highly sensitive to azimuth attitude sensitive errors.
- The rms X- and Z-accelerometer scale factor pitch attitude sensitivity errors were reduced to 7.1 ppm (i.e., total magnitude of 10 ppm). This change arises because, according to Ref. 7, these error terms are now dynamically compensated by the IMU software. According to RI (Ref. 14) the rms residual errors of these terms are less than 10 ppm.

Group 17: Gyro Thermal Transient Drift (Table 2.3-3) - A new magnitude and time constant were recommended by SKD (Ref. 17) for the gyro thermal transient drift error. Because of the smaller time constant (originally 600 sec), the effect of this error group will be diminished.

Groups 18 and 19: Accelerometer Nonlinearities (Table 2.3-3) - SKD has pointed out (Ref. 17) that the second-order and third-order accelerometer nonlinearities are ten times larger in high gain than in low gain. With this change these error groups will become significant contributors to calibration inaccuracies.

Group 24: Gyro Randomness (Table 2.3-3) - The gyro randomness error model used by TASC assumes a random walk (Ref. 10). The growth rate has been adjusted to yield the same error growth over periods of up to ten minutes (the maximum LSF filter period) as the SKD markov model presented at the February 1977 IMU Verification Meeting (Ref. 18) and is equivalent to a variance of 3×10^{-6} $(\text{deg/hr})^2/\text{hr}$. (The ramp model presented in Ref. 18 is insignificant over periods of up to one hour, relative to attitude sensitive and thermal transient drifts.)

More recently, SKD has developed a new gyro randomness model based on IMU test data (Ref. 19). Preliminary calculations performed by TASC indicate that the average LSF filter estimation errors for filtering times of up to 50 minutes (the maximum estimation period) with the SKD model would exceed those with the current TASC model (Ref. 4) by some 22%. Since additional information on the SKD model has not yet been obtained, the TASC model has been retained.

Group 25: Accelerometer Output Noise (Table 2.3-3)

The accelerometer output noise model consists of a markov process and a quantization error. The markov process has an rms error level of 5 μg and a correlation time of 0.4 sec (Ref. 1). The velocity quantization error with the accelerometers operating in the low gain mode is determined as follows:

$$\text{One } \Delta V \text{ pulse} = 0.0344 \text{ fps} \qquad (2.3\text{-}4)$$

Each time an element of the final velocity vector is sampled, quantization contributes an error ranging from -0.0172 fps to +0.0172 fps. Assuming that this total velocity error is independent from velocity sample to velocity sample, each ΔV pulse count has a random error selected from a triangular distribution shown in Fig. 2.3-1. Although the total velocity error

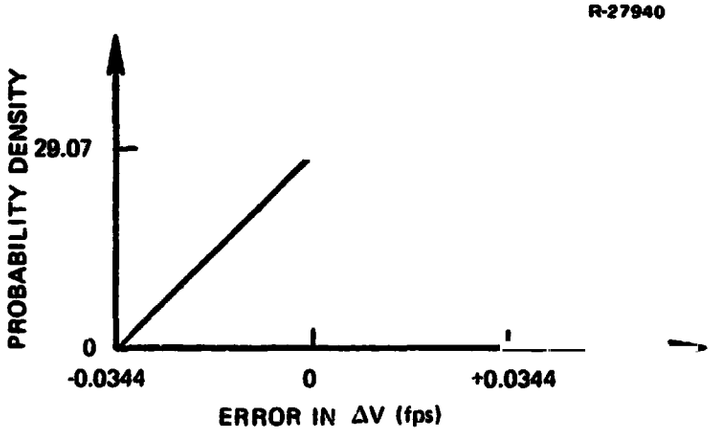

Figure 2.3-1 Error in a ΔV Pulse Count Due to Quantization

due to quantization is independent from sample to sample, the ΔV pulse count errors are correlated from sample to sample. Due to the nongaussian nature of this error source, a simplified monte carlo simulation tool is used to support the evaluation of its contribution to calibration and alignment errors (Ref. 20).

The quantization level for the resolvers is 20 $\widehat{\text{sec}}$. Because dithering rates are applied to all axes along which successive resolver measurements are made, this quantization error may be represented as an uncorrelated measurement noise with

$$R_{11_{ii}} = (20)^2/12 = 33.3\ (\widehat{\text{sec}})^2 \qquad (2.3\text{-}5)$$

The vehicle motions model was specified in detail in Ref. 1. The equivalent state space representation of this effect is

$$\begin{bmatrix} \underline{x}_W \\ \underline{x}_V \end{bmatrix} = \begin{bmatrix} A & 0 \\ B & C \end{bmatrix} \begin{bmatrix} \underline{x}_W \\ \underline{x}_V \end{bmatrix} + \begin{bmatrix} K \\ 0 \end{bmatrix} \begin{bmatrix} \underline{N} \end{bmatrix} \qquad (2.3\text{-}6)$$

where

$$\underline{x}_W = \begin{bmatrix} \text{North wind velocity} \\ \text{West wind velocity} \\ \text{West wind acceleration} \end{bmatrix} \qquad (2.3\text{-}7)$$

$$\underline{x}_V = \begin{bmatrix} \text{North IMU displacement} \\ \text{North IMU velocity} \\ \text{West IMU displacement} \\ \text{West IMU velocity} \\ \text{Vertical IMU displacement} \\ \text{Vertical IMU velocity} \end{bmatrix} \qquad (2.3\text{-}8)$$

$\underline{N}$ is a white, gaussian random process and A, B, C and K are defined in Ref. 1. Since in the OFT mission both the Hangar and the Preflight calibration are performed on the launch pad, the same vehicle motion model is used for both cases. The IMU velocity induced by vehicle motions is modeled as a measurement error source for the LSF filter since the filter uses successive velocity measurements to derive IMU accelerations and acceleration rates.

2.3.3 Reliability of IMU Error Model and Data Base

The majority of the error terms summarized by Tables 2.3-2 through 2.3-4 are based on limited test data. Often the available test data may be from IMUs which do not incorporate the latest hardware and software modifications. This lack of sufficient representative test data may help to explain the fact that major changes of IMU error models have repeatedly been developed, often accompanied by extensive cal/align modifications. These modifications generally consist of costly and/or time consuming hardware and software fixes. A few examples are:

- Two changes in the accelerometer scale factor asymmetry model, i.e., from the model used in the ALT software to that used in the OFT (Ref. 3) software to that recognized by Ref. 7
- Belated recognition that accelerometer nonlinearities (Groups 18 and 19) are 10 times larger in high gain in low gain
- A recently proposed gyro randomness model
- Recent identification of the accelerometer double dead band problem
- Several model and cal/align changes associated with gyro heading and accelerometer attitude sensitive effects.

These changes represent model improvements which are a natural consequence of the growing amount of applicable test data. The following questions, however, are worth asking:

- How many additional model improvements are still to be discovered, and what would be their impact?
- Is the "right kind" of test data being generated to help uncover potentially serious model (or IMU) deficiencies?
- For any additional model deficiencies identified, is it really necessary to make hardware or software modifications?

These questions are highly relevant because any assessment of IMU cal/align performance is ultimately limited by how well the assumed IMU error model matches the actual hardware error mechanisms. Recommendations for minimizing the impact of any IMU model deficiencies encountered subsequent to this cal/align analysis have been discussed with JSC.

2.4 OFT CALIBRATION AND ALIGNMENT PERFORMANCE

The covariance analysis program for the IMU cal/align software includes all major changes to Hangar Coarse Alignment, Hangar Cal A, Preflight Coarse Alignment, Preflight Cal A, and Gyrocompassing as reflected by the 15 December 1978 release of the OFT Level C FSSR (Ref. 6). The error budget presented herein includes all error sources shown in Table 2.3-1 and discussed in Section 2.3 and Ref. 9. The results shown serve to verify the correctness of the cal/align equations specified in the FSSR and identify the dominant error mechanisms for all calibrated IMU parameters.

The error budgets for Hangar Coarse Alignment, Hangar Cal A, Hangar Cal B, and Hangar Cal C are given in Section 2.4.1, and for Preflight Coarse Alignment, Preflight Cal A, Gyrocompassing, and Velocity and Tilt Initialization in Section 2.4.2. In addition, in Section 2.4.3, a more detailed error budget is given for the accelerometer attitude sensitive errors because these are dominant contributors throughout the entire calibration and alignment procedure.

2.4.1 Hangar Calibration Performance

The Hangar cal/align sequences have the following functions:

- Hangar Coarse Alignment - Estimate the IMU case orientation. Table 2.4-1 displays both the rms level error and the azimuth error of this estimate.
- Hangar Cal A - Calibrate a total of 35 gyro and accelerometer error parameters. These parameters are organized into 10 different groups. Table 2.4-1 displays the rms value of the calibration error of all parameters contained in each group. The corresponding column headings are identified by codes similar to those used in Table 2.3-1 (DF=gyro bias drifts, etc.).
- Gangar Cal B - Calibrate 4 resolver error parameters and 2 misalignments of the compensated accelerometer frame with respect to the platform Z (azimuth rotation) axis. These parameters are organized into two groups. Table 2.4-1 displays the rms value of the calibration error of all parameters contained in each group. The groups are accelerometer and gyro misalignments, and resolver offsets and gimbal nonorthogonalities, and the results are headed by 'GROUP 12' and 'GROUP 13', respectively.

CONTRIBUTING ERROR SOURCES			RMS C					
			COARSE ALIGNMENT					
	NAME	MAGNITUDE	LEVEL sec	AZIMUTH sec	DF sec/sec	DI,S,O sec/sec/g	KT ppm	
I.	CALIBRATED IMU ERRORS							
2.	Gyro Bias Drift	0.035 sec/sec	-+	(672.2)	-	-	-	
3.	Gyro Mass Unbalance	≤0.300 sec/sec/g	-	81.6	-	-	-	
4.	Gyro Torquer Scale Factor	400 ppm	-	-	-	-	-	
5.	Gyro Misalignment	120 sec	-	(167.6)	-	-	-	
6.	Accel. Bias - Low Gain	≤200 µg	-	-	-	-	-	
7.	Accel. Scale Factor - Low Gain	200 µg/g	-	-	-	-	-	
8.	Accel. Bias - High Gain	≤200 µg	20.6	-	-	-	-	
9.	Accel. Scale Factor - High Gain	200 µg/g	7.7	-	-	-	-	
10.	Accel. Scale Factor Asymm. - Correlated	200 µg/g	-	10.9	-	-	-	
	- Uncorrelated	30 µg/g	7.7	-	-	-	-	
11.	Accel. Nonorthogonality	60 sec	8.2	-	-	-	-	
12.	Accel. and Gyro Misalignment	60 sec	(59.4)	69.5	-	-	-	
13.	Resolver Offset, Gimbal Nonorthogonality	≤200 sec	(204.8)	(216.8)	-	-	-	
II.	NONCALIBRATED IMU ERRORS							
14.	Gyro Anisoelasticity	≤0.025 sec/sec/g^2	-	129.0	(0.005)	(0.005)	-	
15.	Gyro Output Axis Mass Unbalance	0.005 sec/sec/g	-	94.3	0.004	0.003	-	
16.	Gyro Attitude Sensitive Drift	≤0.008 sec/sec	-	(88.2)	(0.011)	(0.010)	-	
17.	Gyro Thermal Transient Drift	0.01 sec/sec	-	117.2	0.001	0.003	5.2	
18.	Accel. Nonlinearity - 2nd Order	≤150 µg/g^2	4.9	-	0.002	0.002	(81.3)	
19.	Accel. Nonlinearity - 3rd Order	≤ 50 µg/g^3	-	-	-	-	-	
20.	Accel. Attitude Sensitive Bias	≤7.1 µg	-	-	-	-	7.6	2
21.	Accel. Attitude Sensitive Scale Factor	≤ 22 µg/g	3.8	-	0.001	0.001	(23.6)	(4
22.	Outer Roll Offset and Misalignment	200 sec	-	-	-	-	-	
23.	Resolver Harmonic	≤ 20 sec	28.9	28.9	-	-	-	
III.	RANDOM AND QUANTIZATION ERRORS							
24.	Gyro Randomness and Quantization							
25.	Accel. Randomness and Quantization	See Table 2.3-3	-	23.7	0.003	(0.008)	14.1	(4
27.	Vehicle Motion							
26.	Resolver Randomness and Quantization	See Table 2.3-3	13.3	13.3	-	-	-	
	RSS OF ERROR GROUPS 2-27		217.1	784.1	0.013	0.014	86.3	7
	PERFORMANCE SPECIFICATION		1600[1]	1800[2]	0.015	0.025	200	6

+ These error budget contributions are negligible.

† In low gain the error is 0 ppm, in high gain the error is 30 ppm.

* Excluding contributions from Error Group 26 which are not significant.

1. Determined from limits of tilt removal mechanization during calibration
2. Value recommended by Singer-Kearfott.
3. 30 sec for gimbal nonorthgonality.
4. N.S. = Not Specified

FOLDOUT FRAME

TABLE 2.4-1
HANGAR CALIBRATION ERROR BUDGET

T-3270

RMS CALIBRATION ERRORS OF IMU PARAMETERS														
ALIGNMENT	HANGAR CAL A											CAL B		CAL C
AZIMUTH sec	DF sec/sec	DI,S,O sec/sec/g	KT ppm	B sec	KO µg	K1 µg/g	KOH µg	K1H µg/g	KS µg/g	DELT sec	GROUP 12 sec	GROUP 13 sec	LEVEL sec
(672.2)	-	-	-	-	-	-	-	-	-	-	-	-	-
81.6	-	-	-	-	-	-	-	-	-	-	-	-	-
-	-	-	-	-	-	-	-	-	-	-	-	-	-
(167.6)	-	-	-	-	-	-	-	-	-	-	-	-	-
-	-	-	-	-	-	-	-	-	-	-	-	-	-
-	-	-	-	-	-	-	-	-	-	-	-	-	-
-	-	-	-	-	-	-	-	-	-	-	-	-	-
10.9	-	-	-	-	-	-	-	-	-	-	-	-	-
-	-	-	-	-	-	-	30.0	-	(≤30.0)†	-	-	-	8.8
-	-	-	-	-	-	-	-	-	-	-	-	-	-
69.5	-	-	-	-	-	-	-	-	-	-	-	-	-
(216.8)	-	-	-	-	-	-	-	-	-	-	-	-	-
129.0	(0.005)	(0.005)	-	-	-	-	-	-	-	-	-	-	-
94.3	0.004	0.003	-	-	-	-	-	-	-	-	-	-	-
(188.2)	(0.011)	(0.010)	-	-	-	-	-	-	-	-	-	-	-
117.2	0.001	0.003	5.2	-	-	-	-	-	-	-	1.4	-	2.8
-	0.002	0.002	(81.3)	-	18.2	-	(25.3)	-	(29.6)	-	-	-	(36.6)
-	-	-	-	-	3.5	-	(41.5)	-	8.5	-	-	-	12.1
-	-	-	7.6	2.0	(23.1)	5.3	23.1	5.3	23.7	(2.0)	1.3	1.7	7.1
-	0.001	0.001	(23.6)	(6.0)	(69.5)	(16.2)	(69.5)	(16.2)	(69.7)	(5.6)	(4.0)	5.2	21.8
-	-	-	-	-	-	-	-	-	-	-	-	-	-
28.9	-	-	-	-	-	-	-	-	-	-	-	(25.0)	(58.4)
23.7	0.003	(0.008)	14.1	(4.0)	6.4	0.7	6.6	0.4	4.7	0.6	(4.0)	3.5	6.2
13.3	-	-	-	-	-	-	-	-	-	-	(0.5)	(12.7)	*
784.1	0.013	0.014	86.3	7.5	75.8	17.0	154.0	17.0	85.4	6.0	12.1	28.8	74.5
1800[2]	0.015	0.025	200	60	50	40	50	40	40	15	60	≤100[3]	N.S.[4]

FOLDOUT FRAME

- Hangar Cal C - Determine the discrepancies between accelerometer and resolver indication of platform level misalignments and store the difference of these discrepancies between each pair of IMU's. These differences will be computed once again during Gyrocompassing and, when compared against the stored differences, constitute the Gyrocompass Goodness Test.

Table 2.4-1 presents the performance results (both error budgets and overall performance) for these cal/align sequences. For reference, the magnitude of the largest error source* within each error source group is given. The remaining numbers in Table 2.4-1 represent the root-sum-square (rss) of the contribution from all scalar error sources contained in each error source group, specified at the left of the corresponding row, to the calibration or alignment error of the error parameter group specified at the top of each corresponding column. As an example, the largest of the 11 gyro anisoelasticities (Group 14) is 0.025 $\widehat{sec}/sec/g^2$. The rss effect of these 11 errors on gyro drift calibration (DF) is 0.005 $\widehat{sec}$/sec per axis.

For reasons of clarity, error contributions which are negligible are indicated by a dash (-) in Table 2.4-1. These values are all smaller than (most are much smaller than) 10% of the rss value of all error sources given in a particular column. Furthermore, the rss of all encircled numbers in each column is equal to at least 95% of the rss total for that column. Thus the encircled numbers represent dominant contributions to cal/align errors of a parameter group. A summary row near the bottom of Table 2.4-1 shows the combined rss effect of all error groups, i.e., the projected cal/align

*Tables 2.3-2 to 2.3-4 give the magnitudes for all error sources.

performance. These results should be contrasted with the cal/align performance specification indicated in the last row of Table 2.4-1.

Level IMU case alignment errors at the end of Hangar Coarse Alignment are dominated, as expected, by resolver offset, gimbal nonorthogonality, and accelerometer and gyro misalignment. The azimuth coarse alignment error is dominated by west gyro bias drift and, to a lesser degree, by azimuth resolver offset, west gyro attitude sensitive drift (approximately 0.008 $\widehat{sec}$/sec rms), and gyro misalignment toward West. Comparison of the last two rows in Table 2.4-1 indicates that the specified Hangar Coarse Alignment accuracy appears to be achievable.

The present Coarse Alignment results exhibit two significant deviations from those reported in Refs. 4 and 5 for the algorithm defined in the December 1976 OFT Level C FSSR (Ref. 3). In the current Coarse Alignment mechanization, the IMU platform is earth rate compensated, and, therefore, gyro misalignment gives rise to a significant azimuth alignment error. In the earlier mechanization (Ref. 3) the platform was kept inertial, and, therefore, gyro misalignment had no significant effect. Also, the effect of gyro thermal transient drift is larger in Table 2.4-1 than in Ref. 4 because the magnitude assigned to this error source in the error model was increased (see Section 2.3.2).

In Hangar Cal A, the dominant contributors to gyro bias and mass unbalance calibration error are noncalibrated gyro errors, primarily the attitude sensitive gyro drift. Gyro randomness and quantization also contribute significantly to mass unbalance calibration error, with the greatest impact

being on the input axis mass unbalance error*. The gyro scale factor calibration error is dominated by second-order accelerometer scale factor nonlinearity. Accelerometer calibration errors are dominated by the effects of the uncalibrated attitude sensitivity of the accelerometer scale factor, discussed further in Section 2.4.3, and the second-order accelerometer nonlinearity.

Comparison of the last two rows in Table 2.4-1 indicates that, except for low gain accelerometer bias and accelerometer scale factor asymmetry, the specified Hangar Cal A calibration accuracy appears to be achievable. The primary reason for noncompliance lies with accelerometer scale factor attitude sensitive errors.

The present Hangar Cal A results exhibit several significant deviations from those reported in Ref. 4 for the cal/align mechanization described in the December 1976 OFT Level C FSSR. They are:

- The effects of gyro attitude sensitive drift are reduced because the magnitude of this error source was decreased (see Section 2.3.2).
- Gyro thermal transient drift is no longer a dominant error source; this fact owing to the reduction in the time constant of this error source (see Section 2.3.2).
- Accelerometer second- and third-order nonlinearity has become a more important error source for those IMU calibration parameters which are estimated with accelerometers in high gain; this is due to the ten-fold increase of this error

*The contribution of gyro randomness and quantization to input axis mass unbalance error is 0.012 $\widehat{\text{sec}}$/sec/g. The smaller 0.008 $\widehat{\text{sec}}$/sec/g is the rms contribution to all mass unbalance errors.

source in high gain (see Section 2.3.2). This effect is particularly noticeable with gyro torquer scale factor and high gain accelerometer bias calibration errors.

- The dominant effect of accelerometer scale factor attitude sensitive errors on accelerometer calibration has increased even further, in spite of the fact that the magnitudes used for several of these error sources are smaller in the current OFT cal/align performance analysis. This result is not surprising, considering that the former mechanization was specially designed to be insensitive to this error source, whereas the current OFT cal/align mechanization is not. More detailed results on this error source are given in Section 2.4.3.

In Hangar Cal B, resolver randomness errors and quantization contribute significantly to all calibration errors, although resolver offset and gimbal nonorthogonality calibration errors are dominated by uncalibrated resolver harmonic errors. The results in Table 2.4-1 do not differ significantly from those obtained in Refs. 4 and 5. Comparison of the last two rows in Table 2.4-1 indicates that the specified Hangar Cal B calibration accuracy appears to be achievable.

Hangar Cal C errors are dominated by resolver harmonics and, to a lesser degree, by accelerometer second-order nonlinearity and attitude sensitive scale factor errors. The results in Table 2.4-1 do not differ significantly from those obtained in Refs. 4 and 5. There is no performance specification for Hangar Cal C. The Hangar Cal C results are intermediate and will be used for the goodness test in gyrocompassing.

In summary, much of the Hangar Calibration error budget appears to be dominated by the uncalibrated accelerometer scale factor attitude sensitivity. In view of the importance of this error source, further discussions of its impact are provided in Section 3.4.3. The gyro scale factor and high gain acceleromter bias calibration errors are dominated by second-order accelerometer nonlinearity. The gyro bias and mass unbalance calibration errros are dominated by gyro attitude sensitive drift and, in the case of input axis mass unbalances, also by gyro randomness.

2.4.2 Preflight Calibration and Alignment Performance

The Preflight cal/align sequences have the following functions:

- Preflight Coarse Alignment - Estimate the IMU case orientation. Table 2.4-2 displays both the rms level error and the azimuth error of this estimate.
- Preflight Cal A - Calibrate a total of 18 gyro and acceleromter error parameters. Table 2.4-2 displays the rms values of all error groups calibrated in this sequence. The other error groups which were calibrated in Hangar Cal A but not in Preflight Cal A are also included for reasons of clarity.
- Gyrocompassing - Estimate the platform azimuth misalignment and perform a goodness test. Table 2.4-3 displays the rms values of the level and azimuth errors expected during the goodness test, as well as the rms value of the azimuth alignment error.
- Velocity and Tilt Initialization - Perform a final level alignment of the IMU and provide a transition period before lift-off. Table 2.4-3 exhibits the level and azimuth misalignment error at the end of Velocity and Tilt Initialization.

CONTRIBUTING ERROR SOURCES			COARSE ALIGNMENT			
	NAME	TURN-OFF TURN-ON INCREMENT	LEVEL sec	AZIMUTH sec	DF sec/sec	DI† sec/
I.	CALIBRATED IMU ERRORS					
2.	Gyro Bias Drift	0.035 sec/sec	-+	672.5	-	-
3.	Gyro Mass Unbalance	0.025 sec/sec/g	-	91.7	-	0.
4.	Gyro Torquer Scale Factor	100 ppm	-	-	0.001	0.
5.	Gyro Misalignment	60 sec	-	83.8	0.002	0.
6.	Accel. Bias - Low Gain	50 µg	-	-	-	-
7.	Accel. Scale Factor - Low Gain	100 ppm	-	-	-	-
8.	Accel. Bias - High Gain	50 µg	10.3	-	-	-
9.	Accel. Scale Factor - High Gain	100 ppm	3.9	-	-	-
10.	Accel. Scale Factor Asymm. - Correlated	20 ppm	5.6	-	-	-
	- Uncorrelated	0 ppm				
11.	Accel. Nonorthogonality	21 sec	2.9	-	-	-
12.	Accel. and Gyro Misalignment	15 sec	14.9	17.4	-	-
13.	Resolver Offset, Gimbal Nonorthogonality	≤20 sec	20.0	20.0	-	-
II.	NONCALIBRATED IMU ERRORS					
14.	Gyro Anisoelasticity	0	-	91.8	0.005	0.0
15.	Gyro Output Axis Mass Unbalance	0	-	19.5	0.003	0.
16.	Gyro Attitude Sensitive Drift	0	-	309.8	0.011	0.
17.	Gyro Thermal Transient Drift	0	-	104.4	0.004	0.
18.	Accel. Nonlinearity - 2nd Order	0	25.9	34.8	0.002	0.
19.	Accel. Nonlinearity - 3rd Order	0	8.5	8.4	-	-
20.	Accel. Attitude Sensitive Bias	0	4.6	5.0	-	-
21.	Accel. Attitude Sensitive Scale Factor	0	14.2	15.4	0.001	0.
22.	Outer Roll Offset and Misalignment	0	-	-	-	-
23.	Resolver Harmonic	0	28.9	28.9	-	-
III.	RANDOM AND QUANTIZATION ERRORS					
24.	Gyro Randomness and Quantization					
25.	Accel. Randomness and Quantization	0	4.2	59.8	0.002	0.00
27.	Vehicle Motion					
26.	Resolver Randomness and Quantization	0	13.3	13.3	-	-
	RSS OF ERROR GROUPS 2-27		52.7	768.2	0.014	0.02
	PERFORMANCE SPECIFICATION		1600[1]	1800[2]	0.015	0.02

‡ These error groups are not calibrated during Preflight Cal A.

+ These error budget contributions are negligible.

† In low gain the error is 20 ppm, in high gain the error is 36.1 ppm.

1. Determined from limits of tilt removal mechanization during calibration.
2. Value recommended by Singer-Kearfott.
3. N.S. = Not Specified.

FOLDOUT FRAME

TABLE 2.4-2
PREFLIGHT CALIBRATION ERROR BUDGET

T-3271

RMS CALIBRATION ERRORS OF IMU PARAMETERS													
ARSE ALIGNMENT		PREFLIGHT CAL A											
EVEL sec	AZIMUTH sec	DF sec/sec	DI†,S,O sec/sec/g	KT‡ ppm	B‡ sec	KO µg	K1 µg/g	KOH µg	K1H µg/g	KS‡ µg/g	DELT‡ sec	GROUP 12‡ sec	GROUP 13‡ sec
-+	(672.4)	-	-	-	-	-	-	-	-	-	-	-	-
-	91.7	-	(0.016)	-	-	-	-	-	-	-	-	-	-
-	-	0.001	0.001	(100)	-	-	-	-	-	-	-	-	-
-	83.8	0.002	0.003	-	(60.)	-	-	-	-	-	-	-	-
-	-	-	-	-	-	-	-	-	-	-	-	-	-
-	-	-	-	-	-	-	-	-	-	-	-	-	-
-.3	-	-	-	-	-	-	-	-	-	-	-	-	-
3.9	-	-	-	-	-	-	-	-	-	-	-	-	-
5.6	-	-	-	-	-	(20.0)	-	36.1	-	(<36.1)†	-	-	-
2.9	-	-	-	-	-	-	-	-	-	-	(21.0)	-	-
(.9)	17.4	-	-	-	-	-	-	-	-	-	-	(15.0)	-
(20.0)	20.0	-	-	-	-	-	-	-	-	-	-	-	(20.0)
-	91.8	(0.005)	(0.005)	-	-	-	-	-	-	-	-	-	-
-	19.5	(0.004)	0.003	-	-	-	-	-	-	-	-	-	-
-	(309.8)	(0.011)	(0.010)	-	-	-	-	-	-	-	-	-	-
-	104.4	(0.004)	0.003	5.2	-	-	-	-	-	-	-	1.4	-
(25.9)	34.8	0.002	0.002	(81.3)	-	18.2	-	(125.3)	-	(29.6)	-	-	-
8.5	8.4	-	-	-	-	3.5	-	(41.5)	-	8.5	-	-	-
4.6	5.0	-	-	7.6	2.0	23.1	5.3	23.1	5.3	23.7	2.0	1.3	1.7
(4.2)	15.4	0.001	0.001	23.6	6.0	(69.5)	(6.2)	(69.5)	(6.2)	(69.5)	5.6	4.0	5.2
-	-	-	-	-	-	-	-	-	-	-	-	-	-
(28.9)	28.9	-	-	-	-	-	-	-	-	-	-	-	(25.0)
4.2	59.8	0.002	(0.007)	14.1	4.0	6.6	0.7	6.6	0.4	4.7	0.6	4.0	3.5
(3.3)	13.3	-	-	-	-	-	-	-	-	-	-	(10.5)	(12.7)
?.7	768.2	0.014	0.022	132.1	60.5	78.4	17.1	155.3	17.1	87.6	21.8	19.3	35.0
-1	1800[2]	0.015	0.025	N.S.[3]	N.S.	50	40	50	40	N.S.	N.S.	N.S.	N.S.

FOLDOUT FRAME 2

TABLE 2.4-3

PREFLIGHT FINE ALIGNMENT ERROR BUDGET

T-3272

CONTRIBUTING ERROR SOURCE GROUPS		RMS VELOCITY ERRORS				
		GYROCOMPASSING			VELOCITY AND TILT INIT.	
NAME		GOODNESS TEST LEVEL sec	GOODNESS TEST AZIMUTH sec	AZIMUTH ALIGN sec	LEVEL ALIGN sec	AZIMUTH ALIGN sec
I. CALIBRATED IMU ERRORS						
2. Gyro Bias Drift		2.1	-*	-	-	-
3. Gyro Mass Unbalance		-	-	6.8	-	21.8
4. Gyro Torquer Scale Factor		-	-	-	-	1.0
5. Gyro Misalignment		-	-	-	-	1.9
6. Accel. Bias	- Low Gain	-	-	-	-	-
7. Accel. Scale Factor	- Low Gain	-	-	-	-	-
8. Accel. Bias	- High Gain	-	-	-	-	-
9. Accel. Scale Factor	- High Gain	-	-	-	-	-
10. Accel. Scale Factor Assym.	- Correlated - Uncorrelated	5.8	3.1	2.4	4.1	2.7
11. Accel. Nonorthogonality		-	-	-	-	-
12. Accel. Gyro Misalignment		21.2	-	-	15.0	-
13. Resolver Offset, Gimbal Nonorthogonality		28.3	28.3	-	-	-
II. NONCALIBRATED IMU ERRORS						
14. Gyro Anisoelasticity		-	2.7	4.0	-	12.3
15. Gyro Output Axis Mass Unbalance		-	-	-	-	-
16. Gyro Attitude Sensitive Drift		-	440.0	311.5	-	112.5
17. Gyro Thermal Transient Drift		-	4.0	2.9	1.4	5.2
18. Accel. Nonlinearity - 2nd Order		-	28.5	20.1	3.7	20.1
19. Accel. Nonlinearity - 3rd Order		-	-	-	-	-
20. Accel. Attitude Sensitive Bias		-	3.8	2.0	4.9	2.0
21. Accel. Attitude Sensitive Scale Factor		-	11.6	6.2	14.9	6.2
22. Outer Roll Offset and Misalignment		-	-	-	-	-
23. Resolver Harmonic		-	-	-	-	-
III. RANDOM AND QUANTIZATION ERRORS						
24. Gyro Randomness and Quantization 25. Accel. Randomness and Quantization 27. Vehicle Motion		1.6	22.5	15.6	4.3	18.5
26. Resolver Randomness and Quantization		*	*	-	-	-
RSS OF ALL ERROR GROUPS		36.3	442.6	312.7	22.8	314.8
RSS OF ALL ERROR GROUPS ASSUMING PERFECT COMPENSATION OF GROUP 16		36.3	48.0+	27.5†	22.8	38.3†
PERFORMANCE SPECIFICATION		40	89	60	20	N.S.[1]

* These error budget contributions are negligible.

" Excluding contributions from Error Group 26 which are not significant.

† Assuming perfect heading sensitivity compensation.

1. N.S. = Not Specified.

Tables 2.4-2 and 2.4-3 summarize the performance results (both error budgets and overall performance) for these cal/align sequences. Most entries in these tables are analogous to those of Table 2.4-1. In addition, Table 2.4-2 shows the largest turn-off turn-on increment magnitude in each error source group.* These error increments are added in an rss sense to the residual calibration errors at the end of Hangar calibration. The salient features of the Preflight cal/align performance evaluation results are discussed below.

Level IMU case alignment errors in Preflight Coarse Alignment are dominated primarily by second-order accelerometer nonlinearity and by resolver harmonic, offset, and nonorthogonality: while azimuth aligment errors are dominated by the turn-off turn-on increment in gyro bias drift and by gyro attitude sensitive drift. Note that the contribution of accelerometer second-order nonlinearity, accelerometer scale factor attitude sensitivity, and gyro attitude sensitive drift to Preflight Coarse Alignment errors is greater than the corresponding contribution in Hangar Coarse Alignment, due to their influence on Hangar Cal A calibration errors (Table 2.4-1). Comparison of the last two rows of Table 2.4-2 indicates that the specified Preflight Coarse Alignment accuracy appears to be achievable.

The present Coarse Alignment results exhibit two significant deviations from those reported in Refs. 4 and 5 for the algorithm defined in the December 1976 OFT Level C FSSR (Ref. 3). The level alignment accuracy is now dominated by the second-order accelerometer nonlinearity, owing to the ten-fold increase of this error source. The azimuth alignment error increased substantially, owing to the increase in the gyro bias drift turn-off turn-on instability.

*Tables 2.3-2 to 2.3-4 give the magnitudes for all error sources.

The Preflight Cal A error budget is similar to the Hangar Cal A error budget, with two noticeable differences: First, the IMU errors which are calibrated in Hangar Cal A but not recalibrated in Preflight Cal A (* in Table 3.4-2) show degradation due to turn-off turn-on instabilities. In most such cases these instabilities dominate the error budget. Second, since accelerometer scale factor asymmetry is not recalibrated, its turn-off turn-on instability contributes directly to accelerometer bias calibration error.

Comparison of the last two rows in Table 2.4-2 indicates that except for low and high gain accelerometer bias, the specified Preflight Cal A accuracy appears to be achievable. The primary reason for noncompliance lies with the accelerometer scale factor attitude sensitive error.

The IMU remains on after Preflight Cal A, which insures against parameter shifts due to power turn-off turn-on. The salient features of the Preflight Alignment performance evaluation results are discussed below.

The Gyrocompass Goodness Test error budget is presented in Table 2.4-3 in the form of rms relative level and azimuth IMU misalignment errors. The level channels of the goodness test are affected primarily by turn-off turn-on instabilities. In the azimuth channel (with the baseline assumption that perfect compensation is achieved for gyro attitude sensitive drifts, resolver offset, and gimbal nonorthogonality), second-order accelerometer nonlinearity and gyro randomness would be the dominant error sources. However, the accuracy of the azimuth axis goodness test is extremely sensitive to gyro attitude sensitive drift compensation errors. For example, if no compensation were applied, the rms accuracy of the relative azimuth misalignment used in the goodness test would degrade to approximately 440 $\widehat{sec}$. Comparison of the

last two rows in Table 2.4-3 indicates that, assuming perfect gyro attitude sensitive drift compensation, the residual values of the goodness test are within the threshold limits specified for that test.

The Gyrocompass azimuth alignment error budget is similar to the azimuth channel of the goodness test, with two notable differences: First, resolver offsets and gimbal non-orthogonalities do not play a role since resolver measurements are not used for azimuth alignment. Second, the statistical effects of most other error sources are reduced by a factor of $\sqrt{2}$ since the goodness test is a comparison of two IMU's while azimuth alignment utilizes measurements from only one IMU. Randomness and quantization errors are significant error contributors in azimuth alignment. As in the azimuth goodness test, there is a strong sensitivity to errors in the gyro heading sensitive drift compensation, yielding a degradation in azimuth alignment error of about 313 $\widehat{\text{sec}}$ in the case of no compensation. In order to achieve the specified azimuth alignment accuracy of 60 $\widehat{\text{sec}}$, approximately 85% of the attitude sensitive drift error at the gyrocompass positions must be removed via special calibration. To insure satisfactory system performance, this calibration should be checked at regular intervals.

Comparison of the last two rows of Table 2.4-3 indicates that the performance specification for azimuth alignment appears to be achievable. This conclusion, however, assumes that near perfect compensation for gyro heading sensitive drifts can be achieved.

The Velocity and Tilt Initialization error budget is also presented in the form of rms level and azimuth alignment

errors. Level alignment errors seem to be dominated by the turn-off turn-on instability in accelerometer misalignments and by accelerometer attitude sensitve errors. The azimuth alignment error budget is similar to that in Gyrocompassing, and the same comments apply with regard to gyro heading sensitive drift compensation. Comparison of the last two lines of Table 2.4-3 indicates that the performance specification for final level alignment appears achievable

In summary, at the end of preflight calibration and alignment, a review of calibration and alignment errors arising from all error sources indicates that:

- The specified calibration accuracies for low and high gain accelerometer biases and for accelerometer scale factor asymmetry are not met on the basis of the current IMU error model. The primary reason for noncompliance lies with the accelerometer scale factor attitude sensitive errors.
- The performance specification for all other IMU cal/align error appears to be acheivable.
- Gyro calibration errors are dominated by turn-off turn-on instabilities.
- Accelerometer calibration errors are dominated by attitude sensitive scale factor errors (discussed further in Section 2.4.3), second-order accelerometer nonlinearity, and turn-off turn-on instability.
- The primary error sources in the baseline Preflight Alignment evaluation are: resolver instabilities in the goodness test, gyro randomness and quantization in the azimuth measurement, and accelerometer misalignment instability and nonlinearity in the level axis measurements.

- The azimuth alignment measurements are extremely sensitive to errors in attitude sensitive gyro drift compensation, yielding rms azimuth alignment errors of 5 $\widehat{\text{min}}$ in each IMU or 7 $\widehat{\text{min}}$ between two IMUs if no compensation is applied. Approximately 85% of this error must be removed via periodic calibration in order to achieve the azimuth alignment specification.

2.4.3 Effect of Accelerometer Scale Factor Attitude Sensitivity

Due to the importance of the accelerometer scale factor attitude sensitivity (error Group 21) in the performance and evaluation results presented in Sections 2.4.1 and 2.4.2, a more detailed error budget for this error group is presented here.

A detailed error budget, showing the contribution of each accelerometer scale factor attitude sensitivity parameter to each accelerometer calibration error in Hangar Cal A is shown in Table 2.4-4. Each row of the table represents an individual error in Group 21, and each column represents an individual accelerometer calibration error in one of Groups 6 to 10. (The high gain results are identical to the low gain results.)

As can be seen in Table 2.4-4, the accelerometer bias and asymmetry calibration errors are affected to much greater degree than are the scale factor calibration errors. The largest error contributions come from the X accelerometer roll gimbal sensitivity, followed by the Z accelerometer azimuth gimbal sensitivity.

TABLE 2.4-4

DETAILED ERROR BUDGET FOR
ERROR GROUP 21 IN HANGAR CAL A

T-3273

ACCEL. AXIS	GIMBAL	ERROR TERM*	RMS ERROR (μg/g)	GROUPS 6,8 KOX,KOY,KOZ (μg)			GROUPS 7,9 K1X,K1Y,K1Z (μg/g)			GROUP 10 KS (μg/g)		
				KOX	KOY	KOZ	K1X	K1Y	K1Z	KSX	KSY	KSZ
X	Roll	cos (2φ)	13.4	-	(46)	(-46)	(-13)	-	-	-	(46)	(-46)
		sin (2φ)	13.4	-	-	-	-	-	-	-	-	-
	Pitch	cos (2θ)	7.1	(-13)	(-31)	(31)	(13)	-	-	(-13)	(-31)	(31)
		sin (2θ)	7.1	6	-	-	-3	-	-	9	-	-
	Azimuth	cos (2ψ)	11.5	(-26)	12	-12	(-11)	-	-	(-26)	12	-12
		sin (2ψ)	11.5	(13)	(18)	(-18)	-2	-	-	11	(18)	(-18)
Y	Roll	cos (2φ)	3.4	12	-	-12	-	3	-	(12)	-	-12
		sin (2φ)	3.4	-	-	-	-	-	-	-	-	-
	Pitch	cos (2θ)	6.7	-7	(-15)	7	-	(-6)	-	-7	(-15)	7
		sin (2θ)	6.7	-	-3	-	-	-1	-	-	-4	-
	Azimuth	cos (2ψ)	11.5	(-27)	11	(27)	-	(-11)	-	(-27)	11	(27)
		sin (2ψ)	11.5	(18)	13	(-18)	-	2	-	(18)	11	(-18)
Z	Roll	cos (2φ)	6.7	-	-	-7	-	-	-	-	-	-
		sin (2φ)	6.7	-	-	-	-	-	-	-	-	-
	Pitch	cos (2θ)	7.1	9	-9	(16)	-	-	-	9	-9	(22)
		sin (2θ)	7.1	-	-	-	-	-	3	-	-	-
	Azimuth	cos (2ψ)	11.0	(-38)	(38)	-	-	-	(11)	(-38)	(38)	-
		sin (2ψ)	11.0	-	-	-	-	-	-	-	-	-
RSS of Error Group 21				62	75	71	22	13	11	62	75	73

* φ = roll, θ = pitch, ψ = azimuth

Because of the overwhelming effect of the accelerometer attitude sensitive errors it was decided (see Ref. 7) to dynamically compensate these errors within the IMU software. Given this situation, it is of interest to know how small the residual attitude sensitivity errors (after compensation) have to be in order that this error source ceases to be a dominant contributor to cal/align errors. To help answer this question, the error budget contributions in Table 2.4-4 were normalized by dividing

these by the magnitude of the corresponding error sources; the latter are also shown in Table 2.4-4. The result of this operation is shown in Table 2.4-5 which contains the factors by which an error source is amplified to determine its contribution to a calibration error. A similar table was constructed for the accelerometer bias attitude sensitivity errors which, as per Ref. 7, will also be compensated within the IMU software. Table 2.4-6 contains the corresponding error amplification factors.

In Table 2.4-5 it can be seen that error amplification factors as high as 4.4 and 4.7 occur several times. The highest factor in Table 2.4-6 is 3.4. Information on these amplification factors was provided to RI to help them specify accuracy requirements for the dynamic compensation of accelerometer attitude sensitivity.

The amplification factors shown in Table 2.4-5 and 2.4-6 depend strongly on the particular platform positions used for calibration purposes. The fact that many of these factors are so large is an indication that the current cal/align mechanization is highly sensitive to accelerometer attitude sensitive errors.

2.4.4 Needs for IMU Error Model Improvement

The results discussed in Section 2.4 clearly identify a number of error sources which are important contributors to cal/align performance. The mathematical models used for these error sources are described in Section 2.3. However, as pointed out in Section 2.3.3, the majority of these models are based on limited test data and, therefore, may not accurately reflect the actual size and characteristics of the corresponding error mechanisms. Thus, future projections of cal/align perform-

TABLE 2.4-5

ERROR AMPLIFICATION FACTORS FOR
ERROR GROUP 21 IN HANGAR CAL A

T-3274

ACCEL. AXIS	GIMBAL	ERROR TERM*	RMS ERROR (μg/g)	GROUPS 6,8 KO,KOH (μg)			GROUPS 7,9 K1,K1H (μg/g)			GROUP 10 KS (μg/g)		
				KOX	KOY	KOZ	K1X	K1Y	K1Z	KSX	KSY	KSZ
X	Roll	cos (2φ)	13.4	-	3.4	-	-1.0	-	-	-	3.4	-
		sin (2φ)	13.4	-	-	-	-	-	-	-	-	-
	Pitch	cos (2θ)	7.1	-1.8	-1.1	1.3	1.8	-	-	-1.8	-1.1	1.3
		sin (2θ)	7.1	0.9	-	-	-0.4	-	-	1.2	-	-
	Azimuth	cos (2ψ)	11.5	-2.3	-2.3	-3.4	-1.0	-	-	-2.2	-2.3	-3.4
		sin (2ψ)	11.5	1.1	1.6	-	-0.2	-	-	0.9	1.6	-
Y	Roll	cos (2φ)	3.4	3.4	-	-	-	1.0	-	4.0	-	-
		sin (2φ)	3.4	-	-	-	-	-	-	-	-	-
	Pitch	cos (2θ)	6.7	-4.4	-2.3	-1.3	-	-1.0	-	-4.7	-2.2	-1.3
		sin (2θ)	6.7	-	-0.5	-	-	-0.2	-	-	-0.6	-
	Azimuth	cos (2ψ)	11.5	1.1	1.0	3.4	-	-1.0	-	1.7	0.9	3.4
		sin (2ψ)	11.5	1.6	1.1	-	-	0.2	-	2.6	0.9	-
Z	Roll	cos (2φ)	6.7	-3.4	-3.4	-1.0	-	-	-	-4.0	-1.1	-
		sin (2φ)	6.7	-	-	-	-	-	-	-	-	-
	Pitch	cos (2θ)	7.1	4.4	1.1	2.2	-	-	-	-4.7	2.2	3.2
		sin (2θ)	7.1	-	-	-	-	-	0.4	-	-	-
	Azimuth	cos (2ψ)	11.0	-1.1	2.3	-	-	-	1.0	-1.7	2.3	-
		sin (2ψ)	11.0	-1.6	-1.6	-	-	-	-	-2.6	-1.6	-

* φ = roll, θ = pitch, ψ = azimuth

ance can be improved primarily by seeking better models for those error sources which present study has found to be most limiting. The latter includes the following:

- The residual error (after dynamic compensation) of accelerometer scale factor attitude sensitivity (Group 21), because of its dominating effect on acceleromter calibration errors

TABLE 2.4-6

ERROR AMPLIFICATION FACTORS FOR ERROR GROUP 20 IN HANGAR CAL A

T-3275

ACCEL. AXIS	GIMBAL	ERROR TERM*	RMS ERROR (μg/g)	GROUPS 6,8 KO,KOH (μg)			GROUPS 7,9 K1,K1H (μg/g)			GROUP 10 KS (μg/g)		
				KOX	KOY	KOZ	K1X	K1Y	K1Z	KSX	KSY	KSZ
X	Roll	cos (2φ)	13.4	-	3.4	-3.4	-1.0	-	-	-	3.4	-3.4
		sin (2φ)	13.4	-	-	-	-	-	-	-	-	-
	Pitch	cos (2θ)	7.1	-1.0	-2.3	2.3	1.0	-	-	-0.9	-2.3	2.3
		sin (2θ)	7.1	0.5	-	-	-0.2	-	-	0.6	-	-
	Azimuth	cos (2ψ)	11.5	-2.3	1.1	-1.1	-1.0	-	-	-2.2	1.1	-1.1
		sin (2ψ)	11.5	1.1	1.6	-1.6	-0.2	-	-	0.9	1.6	-1.6
Y	Roll	cos (2φ)	3.4	3.4	-	-3.4	-	1.0	-	3.4	-	-3.4
		sin (2φ)	3.4	-	-	-	-	-	-	-	-	-
	Pitch	cos (2θ)	6.7	-1.1	-2.3	1.1	-	-1.0	-	-1.1	-2.2	1.1
		sin (2θ)	6.7	-	-0.5	-	-	-0.2	-	-	-0.6	-
	Azimuth	cos (2ψ)	11.5	-2.3	1.0	2.3	-	-1.0	-	-2.3	0.9	2.3
		sin (2ψ)	11.5	1.6	1.1	-1.6	-	0.2	-	1.6	0.9	-1.6
Z	Roll	cos (2φ)	6.7	-	-	-1.0	-	-	-	-	-	-
		sin (2φ)	6.7	-	-	-	-	-	-	-	-	-
	Pitch	cos (2θ)	7.1	1.3	-1.3	2.2	-	-	-	1.3	-1.3	-
		sin (2θ)	7.1	-	-	-	-	-	0.4	-	3.2	-
	Azimuth	cos (2ψ)	11.0	-3.4	3.4	-	-	-	1.0	-3.4	-	-
		sin (2ψ)	11.0	-	-	-	-	-	-	-	-	-

* φ = roll, θ = pitch, ψ = azimuth

- Second-order accelerometer nonlinearity (Group 11), both in high and low gain, because of its dominati - effect on accelerometer calibration errors and gyrocompass level and azimuth alignment
- Turn-off turn-on errors of input axis gyro mass unbalance (Grou 2), because of their dominating effect on gyrocompass azimuth alignment

- Turn-off turn-on instabilities of accelerometer and gyro misalignments (Group 12), because of their degradation of gyrocompass level alignments
- Gyro randomness and quantization (Group 24), because of their degradation of gyro input axis mass unbalance calibration and gyrocompass azimuth alignment
- The accuracy and stability of the gyro heading sensitive drift compensation, because of its impact on gyrocompass azimuth alignment.

It is recommended that the following steps be taken in relation to the above mentioned dominant error sources:

- Generation and evaluation of test data to verify and/or improve the corresponding error models
- Evaluation of the impact of the improved error models on cal/align performance
- Evaluation of the effect of dominant error sources on orbit insertion accuracy.

2.5 SUMMARY AND CONCLUSIONS

A detailed performance analysis of the Space Shuttle calibration and alignment software has been completed. The software evaluated corresponds to the 15 December 1978 issue of the OFT Level C FSSR. The IMU error models used in this study have been updated with the most recent information available on IMU performance.

2.5.1 Summary of Findings

The performance evaluation of the cal/align software has included two efforts. They are:

- Review of the error models used to represent all potentially important IMU error mechanisms
- Development of an error budget showing the contribution of all modeled error sources to calibration and alignment errors.

The principal findings of both efforts are summarized below.

Analytical evaluation of IMU cal/align performance is limited by the completeness and accuracy of the models used to represent IMU errors. For this reason the present study has included a complete review of IMU error models. The major findings of this effort are as follows:

- The error models for accelerometer scale factor asymmetry, accelerometer nonlinearities, and gyro randomness, as well as several error model parameters, were modified to reflect information obtained from recent IMU test data. The final error model used by TASC in this study was reviewed by SKD personnel.
- Many of the above error model improvements have a significant effect on cal/align performance. Since the need for these model improvements has been identified only recently, there is some concern that there may be other important model deficiencies which have not yet been discovered.

Recommendations for further improvements of IMU error models and, hence, for further improving the confidence of the cal/align performance projections are given in Section 3.2.

The evaluation of the calibration and alignment performance was based upon a covariance analysis of all currently known IMU errors. The major findings of this effort are as follows:

- The specified calibration accuracies for low and high gain accelerometer biases and for accelerometer scale factor asymmetry are not met. The primary reason for noncompliance lies with the accelerometer scale factor attitude sensitive errors.

- The performance specification for all other IMU cal/align errors appears to be achievable.

- Gyrocompass azimuth alignment is extremely sensitive to errors in attitude sensitive gyro drift compensation, yielding rms azimuth alignment errors of 5 $\widehat{\text{min}}$ in each IMU or 7 $\widehat{\text{min}}$ between two IMU's if no compensation is applied. Approximately 85% of this error must be removed via calibration in order to achieve the azimuth alignment specification.

- Gyro calibration errors are dominated by turn-off turn-on instabilities.

- Accelerometer calibration errors are dominated by attitude sensitive scale factor errors, second-order accelerometer nonlinearity, and turn-off turn-on instability.

- The primary error sources in the baseline Preflight Alignment evaluation are: resolver instabilities in the goodness test, gyro randomness and quantization in the azimuth measurement, and accelerometer misalignment instability and nonlinearity in the level axis measurements.

The accelerometer attitude sensitive scale factor errors will be dynamically compensated within the IMU software (c.f. Ref. 7). Test data on the compensated IMU's should be generated and evaluated to develop an error model for the residual attitude sensitive errors. Based on the detailed cal/align error budget generated for the study reported here, TASC has provided NASA and Rockwell International with information

necessary to specify the minimum required performance of the above mentioned compensation.

2.5.2 Recommendations

The majority of the Space Shuttle IMU error models are based on limited test data and, therefore, may not accurately reflect the actual size and characteristics of the corresponding error mechanisms. Thus, estimation of cal/align performance under mission conditions can be improved primarily by seeking better models for those error sources which the present study has found to be most limiting. The latter include:

- Accelerometer scale factor attitude sensitivity after dynamic compensation
- Second-order accelerometer nonlinearity
- Turn-off turn-on instabilities of input axis gyro mass unbalance and accelerometer and gyro misalignments
- Gyro randomness and quantization
- Gyro attitude sensitive drift compensation for the gyrocompass positions.

It is recommended that the following steps be taken in relation to these dominant error sources:

- Generation and evaluation of test data to verify and/or improve the corresponding error models
- Evaluation of the impact of the improved error models on cal/align performance
- Evaluation of the effect of dominant error sources on orbit insertion accuracy.

3. POSTFLIGHT IMU ERROR RECOVERY FOR APPROACH AND LANDING MISSION PHASES

Prior to the initial Space Shuttle Approach and Landing Tests (ALT), NASA's experience with the Shuttle IMUs was gathered from bench tests and hardware/software integration tests. The alignment phase of the bench tests is designed to evaluate IMU alignment under laboratory conditions in absolute terms; however, the calibration phase is designed only to evaluate the repeatability of the calibrated IMU parameters. Atmospheric flight tests such as ALT provide an opportunity to evaluate both the navigation performance achievable with the IMU and the true calibration and alignment uncertainties in a flight environment. This chapter provides assessment of the potential accuracy of postflight IMU error recovery for atmospheric flight tests similar to ALT.

There are two likely benefits of postflight IMU error recovery. The most obvious is to validate the IMU performance (both hardware and software). A second benefit of equal importance is that postflight recovery of inflight IMU alignment errors would provide an accurate attitude reference for evaluating (and calibrating) other Shuttle subsystems such as the air data system. Postflight filtering of flight test data is sufficient for the IMU performance evaluation; however, smoothing of alignment errors is desirable for generating the attitude reference. Although the analysis presented in this chapter is restricted to an evaluation of postflight filtering accuracy, it is possible to make strong inferences on smoother performance based on these results. The ALT mission scenario and system error models used in this study are discussed in Section 3.1. The performance results are presented in Section 3.2.

3.1 MISSION SCENARIO AND SYSTEM ERROR MODELS

There are two principal ingredients of a successful performance test program:

- The test design must be adequate to excite the important error mechanisms.
- The test instrumentation must be accurate enough to measure the resulting performance errors.

Because the dynamic environment for the approach and landing mission phases is benign relative to the environment for the ascent and reentry phases, some IMU error sources (in particular, g-sensitive IMU errors) are not observable from ALT test data. Nonetheless, it is possible to select an ALT trajectory to maximize postflight IMU error recovery. In particular, the duration of the test flight should be sufficient for gyro drifts and acceleromter biases to be estimated, and the trajectory should have enough turning maneuvers to make azimuth misalignments observable.

The ALT test scenario selected for the study satisfies both of the above criteria. The ground track for the trajectory is presented in Fig. 3.1-1, and a mission time line is given in Table 3.1-1. The trajectory closely corresponds in both geometry and time-line to the two-abort captive trajectories described in Ref. 21. The principal differences are that, for simplicity, the takeoff and landing were not simulated (dashed curves in Fig. 3.1-1), and the remainder of the trajectory is at constant velocity (500 fps) and altitude. Measurements taken during takeoff and landing would aid error recovery somewhat, but would not significantly alter the performance results presented in Section 3.2.

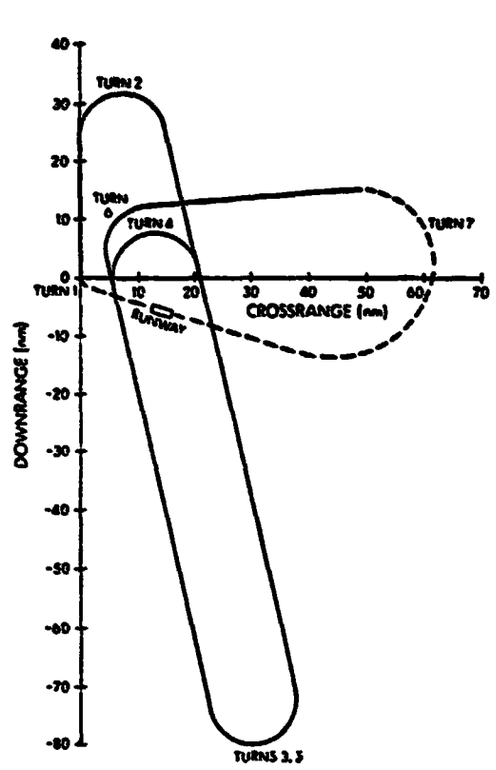

Figure 3.1-1 Ground Track for Sample ALT Trajectory

TABLE 3.1-1
TIME LINE FOR SAMPLE ALT TRAJECTORY

T-0865

EVENT	TIME
Preflight Cal/Align	-60 min
Turn 1 Exit	0
Turn 2 Enter	5 min
Exit	9 min 50 sec
Turn 3 Enter	29 min 10 sec
Exit	33 min 40 sec
Turn 4 Enter	48 min 40 sec
Exit	53 min 10 sec
Turn 5 Enter	68 min 10 sec
Exit	72 min 40 sec
Turn 6 Enter	88 min 40 sec
Exit	91 min 10 sec
Turn 7 Enter	98 min 40 sec

For study purposes, a generalized test instrumentation model that corresponds roughly to photo theodolites in terms of measurement type and accuracy was selected. A position fix of approximately 30 ft accuracy per axis (one sigma) was assumed to be available at 30 sec intervals along the entire trajectory. A summary of the instrumentation error model is presented in Table 3.1-2.

As previously mentioned, ALT trajectories are not sufficiently active to make g-sensitive IMU errors (gyro mass unbalances, accelerometer scale factors, accelerometer asymmetries, etc.) observable. Hence, there is no significant advantage to including these error sources in either a filter or a truth model for ALT postflight error recovery. An exception is the input axis mass unbalance for the z-gyro (vertical input axis). This error source is continually excited by gravity and is indistinguishable from the z-gyro bias drift for ALT.

The IMU error model for the study is presented in Table 3.1-3. The only error sources included are those which are expected to be observable, except that the acceleromter scale factor errors were included to insure that the azimuth misalignment estimate did not become overly optimistic.

TABLE 3.1-2
ASSUMED INSTRUMENTATION ERROR MODEL FOR ALT

MEASUREMENT TYPE	BIAS (1σ)	MEASUREMENT NOISE (1σ)
Position	15 ft	25 ft

TABLE 3.1-3
DATA BASE FOR IMU-RELATED ERROR SOURCES

ERROR SOURCE	STANDARD DEVIATION
Initial Misalignments	
Azimuth	80 $\widehat{\text{sec}}$*
Tilt	20 $\widehat{\text{sec}}$*
Accelerometers	
Biases	50 μg
Scale Factors	100 ppm
Quantization	1 cm/sec
Gyros	
Bias Drifts	0.015 deg/hr
Mass Unbalances	0.025 deg/hr/g

*One hour prior to launch.

The model reflects the nominal prelaunch calibration and alignment performance (see Chapter 2) except that the accelerometer scale factor uncertainty has been increased to account for other effects such as asymmetries and nonlinearities. The IMU errors at completion of the calibration and alignment sequence are modeled as uncorrelated except for a 0.7 correlation coefficient between tilt misalignments and accelerometer biases.

A typical ALT mission plan requires the IMU calibration and alignment sequence to be completed approximately one hour prior to takeoff. The effect of this delay is to introduce an increase in the IMU tilt and azimuth misalignments due to the gyro drifts along the appropriate axes. The delay was accounted for in the simulation by increasing the tilt and azimuth misalignments to 40 $\widehat{\text{sec}}$ and 120 $\widehat{\text{sec}}$, respectively,

and by adding the resulting correlations between alignment and gyro errors.

3.2 ASSESSMENT OF POTENTIAL ERROR RECOVERY PERFORMANCE

The results of a covariance analysis of an optimal postflight processor for the simulated ALT mission are presented in Table 3.2-1 for three times: after the calibration and alignment sequence, at the start of the flight, and at the end of the flight. Because gyro random drift was omitted from the error model, the filtered gyro errors at the start of the flight are the same as at the end of the calibration and alignment sequence.* The accelerometer uncertainties are also constant over this interval, but this is consistent with the complete IMU error model in Chapter 2.

Table 3.2-1 indicates that the ALT measurements are sufficiently accurate to yield a significant reduction in all

TABLE 3.2-1
STANDARD DEVIATIONS OF FILTERED IMU ERRORS
FOR SAMPLE ALT MISSION

T-0478

EVENT	TIME (min)	ERROR SOURCE (1σ)					
		TILT MISALIGNMENT (sec)	AZIMUTH MISALIGNMENT (sec)	LEVEL AXIS GYRO DRIFT (deg/hr)	VERTICAL AXIS GYRO DRIFT* (deg/hr)	ACCELEROMETER BIAS (μg)	ACCELEROMETER SCALE FACTOR (ppm)
Preflight cal/align	-60	20	80	0.015	0.030	50	100
Exit Turn 1	0	40	120	0.015	0.030	50	100
Enter Turn 7	100	11	70	0.002	0.013	40	95

*Includes input axis mass unbalance.

*Gyro random drift is modeled as a random walk which would amount to only 0.006 deg/hr at the end of one hour (see Chapter 2). This would rss to increase the gyro bias drift from 0.015 deg/hr to 0.016 deg/hr.

the level axis errors (tilts, drifts for gyros in the level plane, and acceleromter biases) except for accelerometer scale factor errors. The improvement in the azimuth error estimates (azimuth misalignment and vertical gyro drift) is less dramatic, but the final uncertainty for these parameters is still smaller than it was immediately following the calibration and alignment sequence.

Figure 3.2-1 provides a graph of the IMU misalignment errors as a function of time. As expected, the azimuth uncertainty is reduced by the horizontal accelerations accompanying each turn. Whereas the tilt uncertainty is reduced to a steady state value almost immediately, the azimuth error requires 50 min of flight (three turns) to approach a steady state value. A closer inspection of the data suggests that a standard deviation of 60-70 $\widehat{\text{sec}}$ may be the smallest azimuth error attainable with ALT measurements, primarily because of velocity errors attributable to accelerometer quantization.

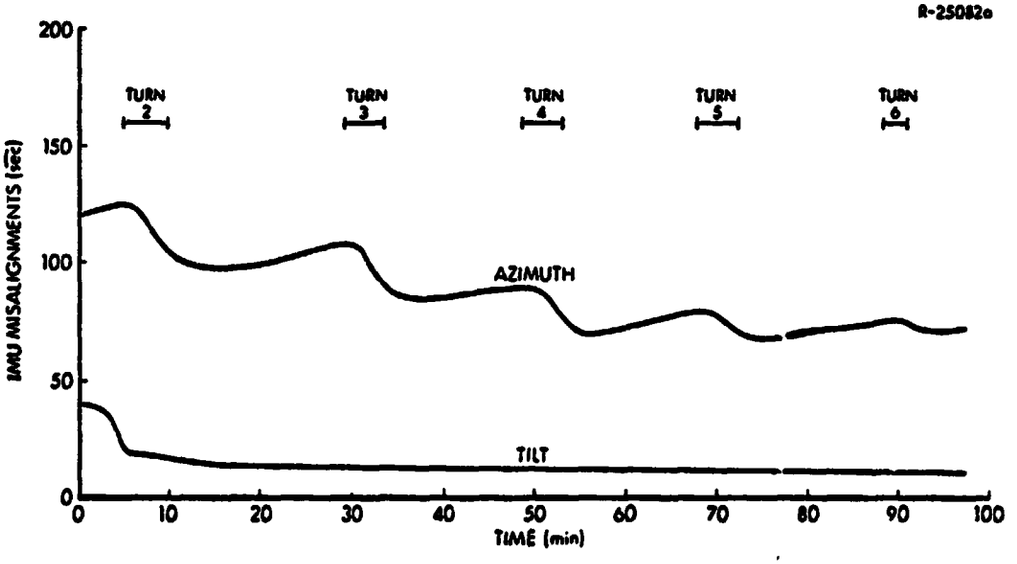

Figure 3.2-1 Filtered IMU Misalignments for Simulated ALT Mission

In addition to the fact that some errors (such as accelerometer scale factor) are unobservable for ALT because they generate small position errors in the ALT environment, other errors are nonseparable because two or more error sources have similar dynamic effects in a one-g environment. Gyro bias drift and input axis mass unbalance for the vertical axis gyro provide one example - the ALT instrumentation measures the sum of the navigation error due to these two error sources and thus the error estimates generated from postflight analysis will be highly correlated. Similarly, the final tilt and accelerometer bias estimates will be almost perfectly correlated. For the error models assumed in this study, the nonseparability of individual error sources is more of a factor in limiting postflight error recovery than the accuracy of the ALT instrumentation set.

Because the gyro and accelerometer errors are constant, the filter performance uncertainties predicted in Table 3.2-1 are the same as the smoother performance would be. Thus, the only estimates which would be improved by smoothing are those for the inflight misalignments - and, for reasons discussed in the preceding paragraphs, it is doubtful that accuracies much better than 60 $\widehat{\text{sec}}$ and 10 $\widehat{\text{sec}}$ can be attained for azimuth and tilt, respectively. Nonetheless, it appears that postflight processing of ALT measurements could maintain IMU alignment errors at a level smaller than the preflight misalignment values. Even with the additional attitude uncertainty associated with the gimbal resolvers (on the order of 30 $\widehat{\text{sec}}$, see Chapter 2), this should provide a useable reference for estimating such attitude-dependent variables as Orbiter angle-of-attack and sideslip angle, and hence for calibrating the air data system.

4. ON ORBIT CALIBRATION OF SHUTTLE IMU ACCELEROMETER AND GYROSCOPE BIASES

4.1 INTRODUCTION AND SUMMARY

A simple calibration of the Shuttle IMU accelerometer and gyroscope biases is planned for orbital operations (Ref. 3). In the very low sensed acceleration environment on orbit, only the instrument biases (as opposed to scale factor errors, etc.) are observable. The on-orbit calibration is an attempt to reduce the likely errors in compensating for these biases to values equivalent to, or better than, those of the last ground calibration, thus mitigating the effects of on-orbit bias instability. Reasonable target values for the accuracy of on-orbit calibration are thus 0.15 deg/hr (1σ) gyro bias and 50 μg (1σ) accelerometer bias (Ref. 22). This chapter examines the likely accuracy of the on-orbit calibration process.

The calibrations for accelerometer biases and for gyro biases are quite different. The accelerometer calibration takes only 320 sec, so that long-term instrument stability is of little importance to the calibration process itself. Also, accelerometer outputs are observed directly by accumulating net delta-velocity pulses, so that instrument measurement errors, except for quantization effects, are negligible. The accelerometer outputs are, however, very sensitive to dynamical disturbances (centripetal acceleration, venting, etc), and these disturbances impose lower limits on the accuracy of accelerometer bias calibration. On the other hand, the duration of the gyroscope calibration is yet to be determined, but it is anticipated to be several hours. The gyro drift cannot be

expected to remain constant during this interval, because of instrument instabilities. While gyro outputs are not appreciably affected by dynamical disturbances, neither is gyro drift directly observable. A star-tracker-to-IMU-cluster alignment procedure must be executed at the beginning and end of the gyro calibration period to assess net gyro drift during the period, and alignment measurement errors are significant. Thus, gyro calibration is largely a tradeoff of instrument stability and measurement error; selecting a calibration period to balance the two will produce the best accuracy.

An important consideration in gyro instrument stability is a type of instability known as heading sensitivity. Heading sensitivity refers to variations in gyro drift rate with a change in cluster-to-IMU-case attitude (see Chapter 2). Also included under the heading sensitivity category are variations in gyro drift rate with the directions the IMU gimbals are rotating and with the direction in which the gyro was last torqued for slewing. These effects have been observed in a one-g ground environment and it is considered likely that they will also exist in a zero-g environment. Accelerometers are also subject to some heading sensitive effects, but these effects are largely scale factor instabilities that are unimportant in the orbital environment.

The following two sections (Sections 4.2 and 4.3) on accelerometer calibration and on gyro calibration consider these processes in more detail. The principal conclusions of this Chapter are presented in Section 4.4.

- Both of the bias calibration processes appear feasible in their proposed forms; no more sophisticated or complex processes are required.

- With mild controls on dynamical disturbances:
  - Thrust to 2 lb. rms or less
  - Vehicle rotation rate to 0.15 deg/sec or less
  - Unpaired impulsive events to 20,000 lb-ft/sec or less

  accelerometer bias calibration accuracy should be better than 20 μg(1σ).

- The amount and effect of heading sensitive gyro drift is very difficult to predict on orbit. Without it, a 16 hr gyro calibration period is optimal, and would be accurate to 0.007 deg/hr (1σ). Any period from 7 hr to 36 hr would yield bias drift rate calibration accuracy of better than 0.01 deg/hr (1σ). With heading sensitive gyro drift, the accuracy of the bias calibration could degrade to 0.02 deg/hr (1σ) or worse.

4.2 ACCELEROMETER CALIBRATION

In accelerometer calibration on orbit, net compensated accelerometer pulses accumulated over a time interval are divided by the interval length to estimate uncompensated accelerometer bias (Ref. 3). The procedure assumes that there is a negligible input to the accelerometers on orbit, so that all of the compensated output represents uncompensated bias effects. Errors in the calibration result from the quantization of the accelerometer output into digital pulses, from disturbing dynamical effects, and (to a lesser extent) from accelerometer attitude sensitivity.

In the low gain mode used for the calibration, one accelerometer pulse represents one milli-g-sec of velocity change. An accelerometer calibration interval of 320 sec is contemplated, so that a one-pulse error would produce a bias estimation error of 3.125 μg. If the precise beginning

and ending times of the calibration were selected without regard to the accelerometer pulse stream itself, and if the accelerometer produced pulses uniformly on orbit, then the rms bias estimation error due to quantization would be only about 40% of the one-pulse error, or about 1.28 μg. Accelerometers, however, do not all behave ideally. Some instruments output pulses in groups of two or more with the same polarity, even for vanishingly low input accelerations. Given that the target accuracy of accelerometer bias compensation is in the 50 μg range, even moderately abnormal quantization effects will not likely prove to be a limiting factor.

Disturbing effects due to vehicle motion are another matter. Any large disturbances would be detected by the unreasonableness of the calibration test results themselves, and moderate disturbing effects localized in time to periods much shorter than 320 sec could be caught by a well designed test that used sub-interval data for reasonableness checks. Some disturbances will have to be controlled or monitored by other means.

A list of likely disturbance sources is:

- Thrust due to gasses venting from the orbiter, possibly for water evaporation (for cooling) or for vehicle attitude control
- Vehicle rotation rates, possibly due to star acquisition for concurrent gyro calibration
- Impulsive events, possibly due to payload shifting or hatch movement.

RMS venting thrusts are currently estimated to be in the 1 lb region (Ref. 23). Assuming a 200,000 lb Orbiter, 1 lb

of thrust gives 5 μg of acceleration, which translates directly into a 5 μg acceleromter bias error during calibration. This small value would be acceptable. Some exceptional venting thrusts can produce unacceptable errors. The use of main attitude control jets for major attitude changes can result in a 30 lb burst of thrust over a 2 min span. Such an event must not be allowed during accelerometer calibration, for it would produce a 56 μg error. In general, 1 lb-min of thrust-times-duration in accelerometer calibration will produce 0.94 μg of bias error.

Vehicle rotations can produce sizeable acceleration errors because the IMU is located about 50 ft from the Orbiter center of mass. Centripetal acceleration is given by the familiar

$$a = \omega^2 r, \qquad (4.2\text{-}1)$$

where ω is the rotation rate, and r is the perpendicular distance from the rotation axis. Assuming the distance to be the maximum, 50 ft, the formula reads

$$a = 473\ \omega^2, \qquad (4.2\text{-}2)$$

with a in μg and ω in deg/sec. Thus, a 0.2 deg/sec rotation rate (that planned for use during star acquisition for on-orbit gyro cal) would produce about 19 μg of error. This amount is not intolerable, but it can probably be avoided.

Impulsive events, unless something is permanently ejected from the Orbiter, come in opposing pairs. Something begins to move, causing an impulsive event, and sometime later it stops, causing the opposing impulsive event. If both of these paired events occur during accelerometer calibration,

they will contribute no error. If accelerometer calibration begins or ends between the pair of events, then errors will occur. Again assuming a 200,000 lb Orbiter, an unpaired impulsive event during accelerometer cal will cause an error of

$$\delta a = p/2059, \qquad (4.2\text{-}3)$$

where δa is in μg and p is the momentum of the impulsive event in lb-ft/sec. Obviously, it takes a substantial impulsive event to cause significant error in the accelerometer calibration process; a 1 ton hatch moved at 5 ft/sec would produce only 5 μg of error.

The only accelerometer instability worthy of note is a heading sensitivity error. The behavior of the accelerometer depends to some extent on the attitude of the cluster relative to the IMU case. Ground calibrations maintain good repeatability by always calibrating with the same sequence of cluster-to-case attitudes. By and large, however, the heading sensitivity for the Orbitor IMU is in the accelerometer scale factors, (see Chapter 2) and they are unexcited on orbit. Heading sensitivity of the biases is in the range of 7.5 μg rms, entirely tolerable for on-orbit calibration.

In summary, it appears that control of disturbing dynamical effects:

- Thrust to an rms value of 2 lb or less
- Vehicle rotation rate to less than 0.15 deg/sec
- Unpaired impulsive events to less than 20,000 lb-ft/sec

will allow accelerometer bias calibration on orbit to a level or roughly 20 μg, as Table 4.2-1 illustrates.

TABLE 4.2-1

SUMMARY OF ON-ORBIT ACCELEROMETER
BIAS CALIBRATION ERRORS

ERROR SOURCE	SOURCE MAGNITUDE	RMS CONTRIBUTION TO CALIBRATION ERROR (μg)
Quantization	2 pulses	2.55
Thrust	2 lbs rms	10.00
Rotation	0.15 deg/sec	10.64*
Impulses	20,000 lb-ft/sec	9.71*
Heading Sensitivity	7.5 μg rms	7.50
RSS TOTAL		19.24

*Peak values for worst geometry

4.3 GYRO CALIBRATION

In gyro calibration on orbit, a measured change in gyro drift angle divided by the time interval over which it accumulated is used to estimate the gyro drift rate bias (Ref. 3). To express the calibration in mathematical terms, assume the calibration period begins with time zero (t=0) and ends a period T later (t=T). In symbols, let:

$\Delta\theta_m$ = measured change in gyro drift angle between t=0 and t=T

$\hat{\dot{\theta}}(T)$ = estimated gyro bias drift rate at test's end, t=T

Then the estimation process is simply

$$\hat{\dot{\theta}}(T) = \Delta\theta_m/T. \qquad (4.3\text{-}1)$$

To proceed, it is necessary to assume some statistical model of gyro drift rate. Ignoring for the moment heading sensitive drift rate effects, a model suitable for on orbit conditions (assuming no sensed acceleration) is:

$$\dot{\theta}(t) = b_{initial} + rt + w(t), \qquad (4.3\text{-}2)$$

where b is the fixed bias drift rate at the initial time, r is a fixed ramp drift rate, and w(t) is a random walk process. It should be noted that the instantaneous drift rate bias for this model is $\dot{\theta}(t)$ itself and the bias to be estimated is the final bias, $\dot{\theta}(T)$.

$$b_{final} = \dot{\theta}(T) \qquad (4.3\text{-}3)$$

The rms error in estimating the bias at the end of the test is then

$$\sigma = E\{[\dot{\theta}(T) - \hat{\dot{\theta}}(T)]^2\}^{\frac{1}{2}} \qquad (4.3\text{-}4)$$

where E is the usual ensemble expectation operator. Without loss of generality, it may be assumed that the gyro drift angle is zero at the beginning of calibration ($\theta(0) = 0$), so that the change in drift angle during the calibration period is just the final value $\theta(T)$. Then write:

$$\Delta\theta_m = \theta(T) + \delta\theta_m, \qquad (4.3\text{-}5)$$

were $\delta\theta_m$ is the measurement error in measuring the <u>difference</u> between drift angles at the beginning and end of the calibration.

The differential equation describing the random walk process in Eq. 4.3-2 is:

$$\dot{w}(t) = n(t), \tag{4.3-6}$$

where n(t) is a Gaussian white noise process with covariance function

$$E\{n(t)n(\tau)\} = \sigma_n^2\, \delta(t-\tau) \tag{4.3-7}$$

where δ is the Dirac delta "function." Also, without loss of generality, it will be assumed that the random walk process is zero at the beginning of the calibration interval ($w(0) = 0$).

Making the reasonable assumption of statistical independence of the random walk white noise and of the gyro drift angle measurement error (from each other and from the deterministic parameters) yields for the mean square estimation error

$$\sigma^2 = (\sigma_m^2 + \sigma_n^2\, T^3/3 + r^2T^4/4)T^2, \tag{4.3-8}$$

where σ_m^2 is the mean square angular error in measuring the drift angle change over the calibration interval, i.e., σ_m^2 is the variance of $\delta\theta_m$.

To evaluate the rms estimation error, σ, and to optimize the calibration interval, T, requires numerical values for σ_m, σ_n, and r. From data provided by Rockwell International (Ref. 24), the per-axis error in measuring IMU alignment by observing two stars with the fixed star trackers is 160 $\widehat{sec}$ rms. Since the difference of two such measurements is used in the calibration to measure the change in drift angle, σ_m^2 depends on the extent to which star tracker errors at two different times are correlated. Because the measurements may be

separated by several hours, a conservative assumption is that the errors are uncorrelated, and thus

$$\sigma_m^2 = 2\ (160\ \widehat{\text{sec}})^2 = 3.95\times10^{-3}\ \text{deg}^2 \qquad (4.3\text{-}9)$$

Singer Kearfott Division selects gyroscopes for Shuttle Orbiter use from a much larger population of gyroscopes by means of a 2 hr and a 17 hr test. The 17 hr test effectively insures that the total uncertainty due to the fixed ramp and random drifts satisfies*

$$(119/13)\ \sigma_n^2 + |14.75r|^2 < (0.013\ \text{deg/hr})^2 \qquad (4.3\text{-}10)$$

Thus, firm limits on the two terms (each assuming that the other is zero) are:

$$r^2 \leq (8.81\times10^{-4}\ \text{deg/hr}^2)^2, \qquad (4.3\text{-}11)$$

$$\sigma_n^2 \leq 1.85\times10^{-5}\ \text{deg}^2/\text{hr}^3. \qquad (4.3\text{-}12)$$

The population of <u>selected</u> gyroscopes is likely to have flat distributions of ramp and white noise intensity paramters, so the mean square values of these parameters will be one third of the maximum square values. To split the error into the two pieces, consider the two extreme cases shown in Table 4.3-1. The rms gyro bias estimation error σ (in deg/hr) may now be written in terms of the test interval T (in hr) directly from Eq. 4.3-8 as follows:

<u>Ramp Case</u>

$$\sigma = (1/T)\ (3.95\times10^{-3} + 6.47\times10^{-8}\ T^4)^{\frac{1}{2}} \qquad (4.3\text{-}13)$$

---

*Assuming the gyro drift rate model of Eq. 4.3-2 and the 17 hr test description of Ref. 25.

TABLE 4.3-1
EXTREME CASES FOR DIVISION OF GYRO ERRORS

MEAN SQUARE VALUE	RAMP CASE	RANDOM WALK CASE
r^2	2.59×10^{-7} deg^2/hr^4	0
σ_n^2	0	6.17×10^{-6} deg^2/hr^3

Random Walk Case

$$\sigma = (1/T)\ (3.95\times10^{-3} + 2.06\times10^{-6}\ T^3)^{\frac{1}{2}} \qquad (4.3\text{-}14)$$

The calibration interval may be optimized for either of these two cases. The results are:

Ramp Case

$$T_{opt} = (4\sigma_m^2/r^2)^{1/4} = 15.7 \text{ hr} \qquad (4.3\text{-}15)$$

Random Walk Case

$$T_{opt} = (6\sigma_m^2/\sigma_n^2)^{1/3} = 15.7 \text{ hr} \qquad (4.3.16)$$

The optimum test periods are identical in the two cases, to the significance shown. They are nearly equal because they happen to be close to the gyro test period of 17 hr used to allocate the errors to one case or the other. If the measurement uncertainty, σ_m, were greater, both optimum test periods would be longer than 15.7 hrs, but the test period for the random walk case would be the longer of the two. The opposite would happen for a smaller measurement uncertainty.

The sizes of the calibration errors in the two cases are not so nearly equal. At the optimum calibration time the rms gyro bias calibration errors are:

Ramp Case

$$\sigma = 0.00565 \text{ deg/hr} \qquad (4.3\text{-}17)$$

Random Walk Case

$$\sigma = 0.00695 \text{ deg/hr} \qquad (4.3\text{-}18)$$

Thus, with a calibration interval of about 16 hrs, a one-sigma gyro bias calibration error should be less than 0.007 deg/hr. It should be noted that the calibration accuracy is fairly insensitive to the calibration period. Assuming the error model statistics (σ_m^2, r, σ_n^2) remain the same, the one-sigma error remains less than 0.01 deg/hr (in either case) for periods from 7 to 36 hrs.

The foregoing analysis ignores the heading sensitive gyro drift effects that are potentially of large impact. Measurements on the prototype Shuttle IMU showed rms variations in drift rate of 0.0120 deg/hr as the cluster-to-case attitude was varied 360 deg about the vertical gyro axis (Ref. 16). Other tests have produced drift rate changes as large as 0.07 deg/hr with cluster-to-case attitude changes. Additionally, drift rate sensitivity to the direction of gimbal rotation and to the direction the gyro was last torqued for slewing have been noted. Software and hardware modifications to reduce the magnitude of these effects have been implemented, but a sizable residual heading sensitive drift will remain.

Since the recommended length of on-orbit gyro calibration (ignoring heading sensitivity errors) is about 10 orbital

periods, it might be expected that substantial averaging of drift rate variations due to cluster-to-case attitude sensitivity would occur. The actual averaging obtained would depend on the details of Orbiter attitude during the calibration period. If the Orbiter were inertially stabilized, cluster-to-case attitude would be constant, and no averaging would occur. Given the lack of hard information on expected magnitudes of heading sensitivity, and given the complex dependence of gyro drift rate on unpredictable cluster-to-case attitude, it is very difficult to assess the impact of heading sensitivity on gyro bias calibration accuracy on orbit. A rough estimate is that the accuracy could degrade to the 0.02 deg/hr (1σ) range.

5. ENTRY AND PRELAND NAVIGATION PERFORMANCE

In Ref. 9, TASC presented results of a study of a candidate baseline navigation filter for the entry, preland, and landing phases of the first Orbital Flight Test Mission (OFT-1). The filter analyzed in that report is very pessimistic in its estimates of initial condition uncertainties and external sensor performance. A revised filter, provided by NASA (Ref. 26) with reworked estimates of initial errors and with less conservative assumptions on sensor performance, was specified for comparison with the filter in Ref. 9. Performance of the revised filter is presented in this chapter.

5.1 REVISED NAVIGATION SCENARIO

The trajectory and measurement schedule for the OFT-1 mission as described in Ref. 9, (see also Volume I, Section 2.2.2) with only a change in the time of initiation of baro-altimeter measurement processing, is assumed for this study (see Table 5.1-1). Previously, the baro-altimeter was switched on at an altitude of 84,000 ft (corresponding to a vehicle speed of Mach 2.2) and temporarily switched off when the vehicle experienced speeds between Mach 1.3 and Mach 0.9. This restriction prevents the processing of this altitude measurement until after the 31,000 ft altitude, and yields a total baro-altimeter operating time of 42 sec as compared to 183 sec for the previous filter.

TABLE 5.1-1
KEY EVENTS FOR OFT-1 MISSION

T-0489a

NAVIGATION PHASE	EVENT	ELAPSED TIME (sec)	TIME TO TOUCHDOWN (sec)	ALTITUDE ABOVE GEOID (ft)	RELATIVE VELOCITY (fps)	RANGE-TO-GO (ft)
ENTRY NAVIGATION PHASE	Entry Interface, T_0	0.0	1630.1	398,837.	24295.	19,600,000.
	First Drag Measurement, T_{DRAG}	188.2	1441.9	282,174.	24399.	15,400,000.
PRELAND NAVIGATION PHASE	First TACAN Measurement, T_{TACAN}	1052.2	577.9	144,780.	7391.	1,425,000.
	Last Drag Measurement	1248.0	382.1	100,263.	3446.	479,000.
	First Baro Altimeter Measurement, T_{BA}	1493.8	136.3	31,230.	745.	67,288.
	First MLS Azimuth, Elevation, & DME Measurements, T_{MLS} (No TACAN Measurement) (No Baro Altimeter)	1536.0	94.1	20,370.	662.	51,000.
LANDING NAVIGATION PHASE	Reduce Filter Dimension, T_{SW} Switch from 3.84 sec Update Cycle to 1.92 sec Update Cycle	1562.9	67.2	13,580.	622.	35,000.
	First Radar Altimeter Measurement, T_{RA} (No MLS Elevation Measurement) Switch from 1.92 sec Update Cycle to 0.16 sec Update Cycle	1622.4	7.7	2,387.	382.	2,700.
	Touchdown	1630.1	0.0	2,293.	315.	0.

The initial filter covariance matrix has been reworked by NASA and may more closely reflect the actual navigation errors at deorbit burn. The previous filter assumed initial position and velocity errors of equal magnitude in each component of position and velocity. However, some components are more difficult to track during orbital operations than others (e.g., downrange position is more difficult to estimate than crossrange position) and the revised filter covariance takes such differences into account. In addition, the initial misalignments specified for the revised filter are somewhat smaller (approximately 0.2 deg) than those used previously (0.25 deg). Table 5.1-2 presents the initial condition uncertainties in the radial, downrange, and crossrange (R,DR,CR) directions. The initial covariance matrix also assumes a -0.9 correlation between downrange position and vertical velocity.

TABLE 5.1-2
INITIAL CONDITION ERRORS FOR REVISED FILTER

T-0811

STATE	R	DR	CR
Position (ft)	2500	25000	2500
Velocity (fps)	26.3	3.3	3.3
Misalignments (mrad)	3.464	3.464	3.464

The navigation filter for the entry through landing phases is a variable dimension Kalman filter with up to 12 states. After T_{SW} (approximately 12,000 ft altitude) it is a 6 state complementary filter. A schedule of filter states is presented in Fig. 5.1-1.

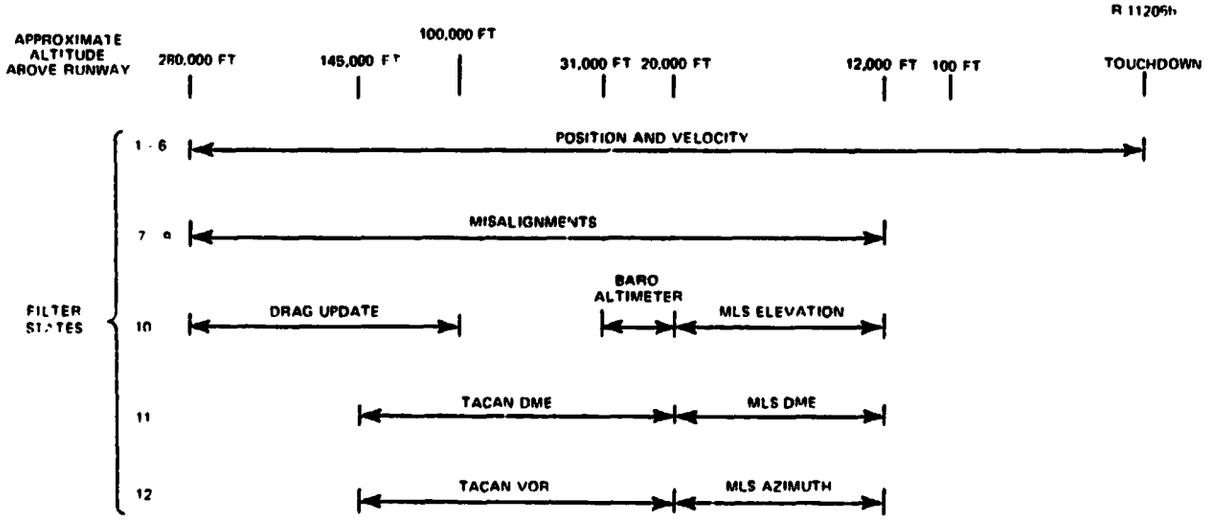

Figure 5.1-1 Schedule for Entry, Preland, and Landing Phase Navigation Filter States

The gain computation algorithm in the Kalman filter mode (i.e., prior to T_{SW}) includes measurement underweighting in order to minimize the possibility of filter divergence:

$$K = PH^T \left[u_{70}HPH^T + R\right]^{-1} \qquad (5.1\text{-}1)$$

where the measurement underweighting factor u_{70} is 1.2 when the rss (filter-indicated) position error is greater than 3280 ft and 1.0 otherwise.

The sensor parameter values for the entry and preland navigation phase Kalman filter are given in Table 5.1-3. The major changes from the filter in Ref. 9 include:

1) A reduction in the rms drag-altitude pseudo-measurement noise from 5148 ft to 2200 ft, and

2) Greatly improved TACAN bearing statistics.

The standard deviation of the TACAN bearing correlated error has been decreased from 29 mrad to 9.64 mrad, and the measurement noise has been halved to 7 mrad.

The baro-altimeter error statistics for the filter are poorer than those used previously, but the baro-altimeter is operated for a much shorter time, thereby diminshing the effects of the poorer performance estimates. The TACAN range parameters are slightly better than, and all the MLS error statistics are exactly the same as, those used in the previous filter.

The time history of the filter-indicated performance between deorbit burn and initiation of the landing phase is summarized in Table 5.1-4. These results represent what optimal performance would be if this 7 state filter model

TABLE 5.1-3

FILTER STATE AND MEASUREMENT ERROR STATISTICS FOR ENTRY AND PRELAND NAVIGATION FILTER

T-0812

MEASUREMENT	CORRELATED ERROR FILTER STATE		MEASUREMENT NOISE
	STANDARD DEVIATION	CORRELATION TIME (SEC)	STANDARD DEVIATION
Drag-Altitude	9842 ft	800	2200 ft
Baro Altimeter	2462 ft	400	868 ft
TACAN DME	444 ft	400	133 ft
TACAN VOR	9.64 mrad	400	7 mrad
MLS DME	80 ft	∞	26 ft
MLS Azimuth	0.96 mrad	∞	0.3 mrad
MLS Elevation	0.96 mrad	∞	0.3 mrad

TABLE 5.1-4

FILTER-INDICATED PERFORMANCE

T-0494-1

EVENT	ELAPSED TIME* (sec)	RMS POSITION ERROR (ft)			RMS VELOCITY ERROR (fps)		
		R	DR	CR	R	DR	CR
Initiation of Deorbit Burn	—	2500	25000	2500	26.3	3.3	3.3
Entry Interface	0.0	16505	24859	8360	38.5	18.5	12.0
	163.2	19540	27289	9628	43.4	20.2	12.0
First Drag Measurement	188.2^{+}	11577	26128	.9809	34.7	16.5	12.0
	1029.1^{+}	9792	29732	28194	33.0	37.9	64.1
First Tacan Measurements	1052.2^{+}	9484	12977	17373	30.4	32.7	52.0
	1489.9^{+}	1966	1182	991	14.2	8.7	11.2
First Baro Altimeter Measurement	1493.8^{+}	1472	901	822	13.9	8.1	10.4
	1536.0^{-}	732	573	262	11.1	8.2	8.0
MLS Acquisition	1536.0^{+}	57	73	65	11.0	6.8	5.6
Initiation of Landing Navigation Phase	1567.9^{-}	44	78	45	2.2	2.5	2.3

*Add 1187.0 sec for elapsed time from deorbit.

were a complete and accurate representation of real-world error dynamics. The major difference from the behavior observed in Ref. 9 is a marked improvement in all components of the predicted position and velocity errors through the period of TACAN-only operation (i.e., 1052.2 sec to 1493.8 sec). This improvement is expected since the TACAN error statistics, particularly bearing, are improved over the previous filter values. At the switch to MLS, however, velocity errors are larger than those previously indicated because of the baro-altimeter's shorter operating time and poorer measurement statistics. At the switch to the landing navigation phase these velocity errors are approximately twice those indicated in Ref. 9.

5.2 NAVIGATION SYSTEM PERFORMANCE

Performance results for the Space Shuttle entry and preland navigation system are summarized in this section in the form of a table showing rms position and velocity errors at specific flight times, and in the form of partial error budgets at the end of the entry phase ($t=T_{TACAN}$) and at the initiation of MLS measurement processing ($t=T_{MLS}$). These tables are based on only those error sources which have been major contributors to navigation performance down to the 29,000 ft altitude in recent TASC studies. In particular these error sources are

- Initial position and velocity errors (Group 1)
- Initial platform misalignments (Group 1)
- Drag-altitude, and TACAN range and bearing measurement noises (Group 1)
- Accelerometer biases (Group 2)
- TACAN range bias (Group 10) and bearing bias (Group 19)

- Baro-altimeter bias, scale factor and static defect (Group 12)
- The 1962 standard atmosphere modeling error (Group 21)

The error magnitudes associated with these error sources are the same as those used in Ref. 9. While several of the additional error sources could become important for a particular filter mechanization, it is reasonable to assume that they would add only a few percent to the overall performance estimates.

Table 5.2-1 presents a time history of position and velocity errors for the revised navigation filter (generated by root-sum-squaring the individual contributions of the error sources listed above). The principal difference from the performance shown in Ref. 9 is an increase in vertical and downrange errors below an altitude of 85,000 ft, presumably because baro-altimeter measurements are suppressed until late in the mission. The initial covariance for the revised entry filter

TABLE 5.2-1
ESTIMATED PERFORMANCE FOR REVISED NAVIGATION FILTER

T-0813

EVENT	ALTITUDE (ft)	ELAPSED TIME* (sec)	RMS POSITION ERROR (ft)			RMS VELOCITY ERROR (fps)		
			R	DR	CR	R	DR	CR
Before First Drag Meas.	287,000	188.2⁻	2119.	11520.	1368.	14.36	2.26	1.69
Before First Tacan Meas.	145,000	1052.2⁻	2626.	12391.	5076.	19.64	9.45	13.97
After First Tacan Meas.	145,000	1052.2⁺	2790.	4279.	14918.	16.61	13.44	29.72
After Last Drag Meas.	100,000	1248.0⁺	4436.	874.	3159	15.86	10.54	22.83
After First Baro Meas.	31,000	1493.8⁺	1865.	835.	1078.	11.91	7.38	8.84
Before First MLS Meas.	20,000	1536.0⁻	829.	807.	366.	11.93	9.64	5.99

*Add 1187.0 sec for Elapsed Time from Deorbit.

is still pessimistic relative to the truth model covariance as is indicated by a comparison of Table 5.2-1 with the filter-indicated performance, Table 5.1-4.

The initial pessimism of the revised filter along with the lower values of predicted drag-altitude pseudo-measurement noise yields larger radial position errors during blackout than were experienced in Ref. 9. This behavior suggests that, for the assumed truth model error magnitudes, the revised filter is overweigting these altitude measurements. Similarly, the immediate increase in crossrange errors with the processing of the first TACAN bearing measurement is due to the fact that the TACAN bearing error statistics in the filter are now smaller than those in the truth model, again leading to possible over-weighting of the bearing measurements. Finally, as discussed in Ref. 9. the large velocity errors are primarily due to the large IMU misalignments.

Table 5.2-2 presents a partial error budget for the entry navigation phase. The only major contributor (as determined in Ref. 9) which is not included is the nonstandard aerodynamics time-varying bias. This error source was a major contributor to the vertical position error, but its importance for this filter would be overshadowed by the contribution from the drag-altitude pseudo-measurement noise. Of the total projected performance values only the vertical position error is considerably different (in this case, worse) than that of the previous filter.

The 5000 ft standard deviation for drag-altitude pseudo-measurement noise used in Ref. 9 corresponds to a 20% random atmospheric density error. Although this number is consistent with values assumed in recent studies (Refs. 27 and 28), inspection of available atmospheric density data (Ref. 29)

TABLE 5.2-2

REVISED PARTIAL ERROR BUDGET FOR THE ENTRY NAVIGATION PHASE

T-0814

ERROR SOURCE	VALUE	RMS NAVIGATION ERROR AT 145,000 ft					
		POSITION (ft)			VELOCITY (fps)		
		R	DR	CR	R	DR	CR
I. FILTER STATES AND MEASUREMENT NOISE							
Initial Condition Errors							
Positions and Velocities	Ref. 9	224.	11100.	3752.	14.75	3.25	2.17
Misalignments	285 sec	150.	970.	2416.	6.07	6.46	13.54
Uncorrelated Measurement Noise							
Altitude	5000 ft	2603.	2037.	1257.	10.61	4.76	1.64
	(1250 ft)	(651.)	(509.)	(314.)	(2.65)	(1.19)	(0.41)
INS Quantization Noise	0.0328 fps	—*	—	—	—	—	—
II. IMU-RELATED STATES							
Accelerometer Errors							
2. Biases	50 μg	220.	1903.	1617.	1.52	1.68	1.22
3. Scale Factors	100 ppm	—	—	—	—	—	—
4. Asymmetries	100 ppm	—	—	—	—	—	—
5. Nonorthogonalities	15 sec	—	—	—	—	—	—
Gyro Errors							
7. Biases Drifts	0.035°/hr	—	—	—	—	—	—
8. Mass Unbalances	0.025°/hr/g	—	—	—	—	—	—
IV. DRAG-RELATED STATES							
21. Non-Standard Density							
1962 Standard Atmosphere Modeling Error	4-Term(<9%) Ref. 9	5.	4649.	1286.	4.06	3.40	1.75
Time-Varying Bias	Winter (<8%)	—	—	—	—	—	—
First-Order Markov	(<6%) Ref. 9	—	—	—	—	—	—
22. Non-Standard Wind							
Westerly	Winter (<295 fps) Ref. 9	—	—	—	—	—	—
Crosswind / Headwind	(<110 fps) Ref. 9	—	—	—	—	—	—
23. Non-Standard Aerodynamics							
Time-Varying Bias	(<9.5%) Ref. 9	—	—	—	—	—	—
First-Order Markov	5% of C_D	—	—	—	—	—	—
Total Projected Performance		2626.	12391.	5076.	19.64	9.45	13.97
Total Projected Performance With Alternate Measurement Noise		(738.)	(12233.)	(4928.)	(16.74)	(8.25)	(13.83)

*Negligible contributor

does not support a value greater than 1250 ft (5%). Because the revised filter is much more sensitive to the magnitude of the drag-altitude pseudo-measurement noise than previous filters, it is desirable to include in Table 4.2-2 the more optimistic (and, perhaps, realistic) vertical channel performance which would be attained with this smaller value. The parenthetical entries in the error budget provide both error contributions and total projected performance with the smaller measurement noise. Even with the lower value of measurement noise, this error source is at least a major contributor to the vertical position error. There is a clear need for adequate test data and a better understanding of this error source.

Except for the contribution of the initial misalignments to the vertical position error, which is much smaller than previously observed, all the remaining contributions listed in Table 5.2-2 are approximately equal to those of the previous filter.

A partial error budget for the revised navigation filter at 20,000 ft is given in Table 5.2-3. Because of a lack of reliable data on TACAN bearing errors, alternate values of the TACAN bearing errors, and the corresponding total projected performance using these alternate values, are also included in the table. The total projected performance in nearly all channels is somewhat poorer than that of the previous filter.

The filter's heavy weighting of the TACAN bearing measurement is indicated by the very large contributions of the TACAN bearing bias and measurement noise to all components of both the position and velocity errors. Even with these error sources set at the lesser values, i.e., 6 mrad bias and

TABLE 5.2-3
REVISED PARTIAL ERROR BUDGET AT 20,000 FT

T-0503-1

ERROR SOURCE	VALUE	RMS NAVIGATION ERROR AT 20,000 ft					
		POSITION (ft)			VELOCITY (fps)		
		R	DR	CR	R	DR	CR
I. FILTER STATES AND MEASUREMENT NOISE							
Initial Conditions							
Positions and Velocities	Ref. 9	29.1	31.5	13.9	4.04	0.25	1.02
Misalignments	285 sec	77.4	103.2	49.7	3.89	1.73	3.93
Uncorrelated Measurement Noise							
TACAN Range	100 ft	141.2	62.1	31.7	1.93	0.57	0.54
TACAN Bearing	12 mrad (6 mrad)	348.7 (174.4)	429.8 (214.9)	133.4 (66.7)	4.61 (2.30)	5.50 (2.75)	1.49 (0.74)
Baro-Altimeter	$0.24\ e^{h/24018}$ ft	— *	—	—	—	—	—
INS Quantization Noise	0.0328 fps	—	—	—	—	—	—
II. INU-RELATED STATES							
Accelerometer							
2. Biases	50 μg	9.5	12.8	6.0	0.65	0.19	0.52
3. Scale Factors	100 ppm	—	—	—	—	—	—
4. Asymmetries	100 ppm	—	—	—	—	—	—
5. Nonorthogonalities	15 sec	—	—	—	—	—	—
Gyro							
7. Bias Drifts	0.035^{o}/hr	—	—	—	—	—	—
8. Mass Unbalances	0.025^{o}/hr/g	—	—	—	—	—	—
IV. EXTERNAL AID-RELATED STATES							
10. TACAN Range Bias	385 ft	449.4	150.6	70.4	4.96	1.90	2.61
11. TACAN Range Scale Factor	100 ppm	—	—	—	—	—	—
12. Baro-Altimeter Errors							
Bias	100 ft						
Scale Factor	3%						
Static Defect	1.52×10^{-4} $ft/ft^2/sec^2$	69.7	34.5	20.4	0.95	0.30	0.50
First-Order Markov	20 ft	—	—	—	—	—	—
16. TACAN Survey Errors	1 ft	—	—	—	—	—	—
19. TACAN Bearing Bias	12 mrad (6 mrad)	575.5 (287.7)	652.8 (326.4)	326.9 (163.4)	7.74 (3.87)	7.46 (3.73)	3.10 (1.55)
1.,21.,22.,23. Drag-Related Errors	Ref. 2	—	—	—	—	—	—
Total Projected Performance		828.5	806.5	365.7	11.93	9.64	5.99
Total Projected Performance With Alternate TACAN Bearing Model		(589.0)	(438.5)	(200.5)	(9.02)	(5.35)	(5.20)

*Negligible contributor

6 mrad measurement noise, they are major contributors to all position and velocity errors. As is the case with the altitude pseudo-measurement noise, the importance of the TACAN bearing errors in this filter underlines the need for a better understanding of the true TACAN bearing error mechanisms and their magnitudes.

The TACAN range errors are major contributors to vertical channel errors. These contributions are somewhat larger than observed for the previous filter, due to the slightly improved TACAN range error statistics and the delayed utilization of the baro-altimeter. The baro-altimeter error sources have been reduced to insignificant contributors because the baro-altimeter is operated for a shorter length of time and the filter has much poorer error statistics than the previous filter.

A principal difference between these results and those of the previous filter is the contributions of the initial position and velocity uncertainties. Where previously this error source was a major contributor to all position and velocity errors, it is now a major contributor to only the vertical velocity error. The revised filter, with the reworked estimates of the initial conditions, does not generate the large misalignment estimation errors seen in Ref. 9. As a result, the mechanism which couples these initial position and velocity uncertainties to the position and velocity errors, through the misalignments, does not produce the substantial error contributions observed in Ref. 9.

The initial misalignments continue to be major contributors to vertical and crossrange velocity errors. This is expected since the initial misalignment estimates were reduced, but are still quite large.

Although error budget runs for all the error sources considered above were made down to touchdown, the corresponding error budget tables are not included here. The changes in these tables from the results observed in Ref. 9 are minimal. The principal change is that the TACAN bearing errors are major contributors to crossrange position and velocity errors throughout the remainder of the flight.

Overall the performance of the revised filter down to the 20,000 ft altitude is somewhat poorer than that indicated for the previous filter, primarily because baro-altimeter measurements are suppressed until late in the mission. At altitudes below 20,000 ft, where MLS- and radar altimeter-related errors dominate, the performance of the two filters would be approximately the same. The revised filter experiences two important differences from the previous baseline filter:

- The altitude pseudo-measurement and the TACAN bearing measurement assume very significant roles during the entry and preland navigation phases.
- The initial position and velocity uncertainties do not yield the large misalignment estimates which plagued the filter in Ref. 9.

It should be further noted that the altitude pseudo-measurement noise and the TACAN bearing errors are not well documented or well understood. Their importance in this candidate filter underlines the need for improved (better understood) error models for these error sources.

6. SUMMARY AND CONCLUSIONS

This volume of this final report presents the results of four distinct study areas in Space Shuttle navigation associated with the baseline navigation system configuration. A brief summary of the major conclusions arrived at in the preceeding four chapters is presented here.

6.1 IMU CALIBRATION AND ALIGNMENT COVARIANCE ANALYSIS

Covariance analysis techniques were applied to develop a detailed error budget for the OFT/IMU calibration and alignment algorithm. Similar results were presented in Refs. 4 and 5, but the present results apply to a revised version of the algorithm (Ref. 3, Dec. 1976) with 13-position Hangar Cal A and 7-position Preflight Cal A sequences designed to avoid transient effects of accelerometer gain switching. Several other changes in procedures and analysis, as are detailed in Chapter 2, are also incorporated.

Complete error budgets for the Hangar and Preflight calibrations are presented. Significant conclusions to be drawn from the error budgets include:

- The specified Hangar Cal A calibration accuracy appears to be achievable, except for low gain accelerometer bias and accelerometer scale factor asymmetry. Accelerometer scale factor errors sensitive to gimbal attitude are primarily responsible for the lack of total compliance.

- The specified Hangar Cal B calibration accuracy appears to be achievable.
- The specified Preflight Coarse Alignment accuracy appears achievable.
- The specified Preflight Cal A accuracy appears achievable, except for low and high gain accelerometer bias. Again, the primary reason for noncompliance lies with the accelerometer scale factor attitude sensitivity.
- The specified Gyrocompass Goodness Test accuracy appears achievable only if the gyro attitude sensitive drift can be essentially perfectly compensated.
- The specified Gyrocompass Azimuth Alignment accuracy appears achievable only if the gyro attitude sensitive drift is almost perfectly compensated.
- The specified Velocity and Tilt Initialization accuracy appears achievable.

A more detailed presentation of conclusions and recommendations for IMU calibration and alignment are to be found within Chapter 2 of this Volume. The principal recommendations are for further validation and improvement of the IMU sensor error model terms that heavily impact both the calibration and alignment procedures and the subsequent Orbiter navigation performance.

6.2 POSTFLIGHT IMU ERROR RECOVERY FOR APPROACH AND LANDING MISSION PHASES

Atmospheric flight tests such as ALT provide an opportunity to evaluate both the navigation performance achievable with the IMU and the true calibration and alignment uncertainties in a flight environment. Postflight recovery of inflight IMU errors, especially platform alignment errors, would provide

an accurate reference for the evaluation of other Shuttle subsystems, such as the air data system. The study of postflight error recovery focuses on the test design, on the test instrumentation, and on the data analysis techniques involved. A computer simulation was created to examine these issues.

The results of the simulation indicate a potential for a significant reduction in the preflight uncertainties of level axis errors (tilts, level drifts, and accelerometer biases). Azimuth axis uncertainties are also reduced, but not so significantly. Certain errors, including accelerometer scale factors, are essentially unobservable, while others, including gyro bias and input axis mass unbalance for the azimuth axis, are inseparable. Nonetheless, it appears that postflight processing of ALT measurements could maintain IMU alignment errors at a level smaller than the preflight misalignment values.

6.3 ON-ORBIT CALIBRATION OF SHUTTLE IMU ACCELEROMETER AND GYROSCOPE BIASES

Accelerometer biases and gyroscope bias drifts may be calibrated in the sensed-acceleration free environment on orbit. A short (320 sec) accelerometer calibration will be accurate to about 20 μg (1σ), provided that certain acceleration producing events (venting, thrusting, rotation, and impulsive events) can be held to what appear to be easily achievable levels. Accelerometer stability itself is of little concern over so short a calibration interval.

On orbit gyroscope calibration, on the other hand, is largely a tradeoff of instrument stability and startracker measurement error, the startrackers being used as the attitude reference for gyroscope calibration. With some uncertainty

engendered by the potential effects of heading sensitive gyro drift, it appears that a 16 hr gyro calibration period would achieve bias drift calibrations to a level of 0.007 deg/hr (1σ). Acceleration effects important in on-orbit accelerometer calibration have no relevance to on-orbit gyro calibration.

6.4 ENTRY AND PRELAND NAVIGATION PERFORMANCE

This study is a revision of previous work (Ref. ?) with some changes in assumptions. The main issue is navigation filter performance in the entry, preland, and landing phases of the first Orbital Flight Test mission. The major changes in assumptions from the earlier study are better drag updating and improved TACAN performance in the present study, but a lowering in the maximum altitude at which the baro altimeter is assumed usable (associated with passage of the Orbiter through Mach 1).

The present results show an increase in vertical and downrange errors below a 85,000 ft. altitude because no baro altimeter measurements are yet available, and a greater dependence on the accuracy of the drag updates. This degraded behavior of the filter continues even down to 2000 ft (the baro altimeter being assumed available at 31000 ft), showing the importance of the early altitude measurements. Because the drag update errors and the TACAN errors are not well documented, and because this revised filter depends so strongly on these errors, a better understanding of the statistical behavior of drag updating and TACAN bearing errors should be pursued.

REFERENCES

1. Jones, H.L., and Lüders, G., "Space Shuttle Navigation Analysis," The Analytic Sciences Corporation, Technical Report No. TR-548-1, December 1975.

2. "ALT Level C Functional Subsystem Software Requirements (FSSR)," Rockwell International, Document No. SD-74-SH-0269, March 1976.

3. "OFT Level C Functional Subsystem Software Requirements (FSSR), Inertial Measurement Unit, "Rockwell International, Document No. SD-76-SH-0013, December 1976.

4. Matchett, G.A., et al., "Quarterly Progress Report for the Period Ending 31 December 1977," The Analytic Sciences Corporation, Technical Report No. PR-1001-15, December 1977.

5. Matchett, G.A., et at., "Quarterly Progress Report for the Period Ending 28 February 1978," The Analytic Sciences Corporation, Technical Report No. PR-1001-18, March 1978.

6. "OFT Level C Functional Subsystem Software Requirements (FSSR), Intertial Measurement Unit," Rockwell International, Document No. SD-76-SH-0013A, December 1978.

7. Kang, Y., "Accelerometer Non-Linearity and Attitude Sensitivity Compensation, Orbiter Software Change Request CR-12976," Rockwell International, 22 August 1978.

8. Matchett, G.A., et al., "Quarterly Progress Report for the Period Ending 31 August 1978," The Analytic Sciences Corporation, Technical Report No. PR-1001-24, October 1978.

9. Jones, H.L., et. al., "Space Shuttle Navigation Analysis," The Analytic Sciences Corporation, Technical Report No. TR-548-2, September 1976.

10. Jones, H.L. and Lüders, G., "Quarterly Progress Report for the Period Ending 31 December 1974," The Analytic Sciences Corporation, Technical Report No. PR-548-6, January 1975.

REFERENCES (Continued)

11. "Product Fabrication Specification, Inertial Measurement Unit," The Singer Company, Kearfott Division, Document No. E100F461E100 Rev. G, December 1976.

12. Epple, R.G.E., "Shuttle IMU Math Model for Real Time Simulation," Rockwell International IL NO. 392-240-76-231, June 1976.

13. Matchett, G.A., "Letter to Bronson Stout, Singer Company, Kearfott Division," The Analytic Sciences Corporation, 27 October 1978.

14. Lüders, G., "Personal Communication with Kang, Y.," Rockwell International, 4 December 1978.

15. Rains, R.G., "Personal Communication with Stout, B.," The Singer Company, Kearfott Division, 25 January 1978.

16. "Orbiter Inertial Measurement Unit (IMU) Heading Sensitivity/Gyrocompassing Study," The Singer Company, Kearfott Division, Document No. Y258A530, September 1976.

17. Rains, R.G., "Personal Communication with Stout, B.," The Singer Company, Kearfott Division, 22 September 1978.

18. Wyrick, R.L., "IMU Verification Meeting Minutes," NASA Johnson Space Center, Houston, Texas, Memorandum No. EG-2/77-30, February 1977.

19. Rains, R.G., "Personal Communication with Stout, B.," The Singer Company, Kearfott Division, 5 January 1979.

20. Matchett, G.A., and Rains, R.G., "Quarterly Progress Report for the Period Ending 31 August 1977, The Analytic Sciences Corporation, Technical Report No. PR-1001-12, October 1977.

21. Jenkins, J.M., "Trajectory Tape Description for ALT Preliminary Reference Mission Captive-Active Two-Abort (Profile No. 1) for Navigation Software Development," Johnson Space Center, IN No. 75-FM-52, July 1975.

22. "Specifications for Inertial Measurement Unit (IMU) -Orbiter," Rockwell International, Document No. MC409-0004, 1 June 1974.

REFERENCES (Continued)

23. Osburn, R., Private communication, NASA Johnson Space Center, Houston, Texas, 18 January 1977.

24. Blucker, T.J., Private communication, NASA Johnson Space Center, Houston, Texas, 17 March 1977.

25. Jones, M.E., "Singer Kearfott Mod II and Mod IIC Gyroflex Gyros", NASA Johnson Space Center, Report No. JSC-11548, August 1976.

26. Eckelkamp, R.E., Johnson Space Center, Personal Communication to H.L. Jones, August 1976.

27. Heck, M. and Mayur, N., "OFT-1 Preliminary Entry Navigation Simulation Results," Johnson Space Center, IN No. 76-FM-65, September 1976.

28. Eckelkamp, R.E., "OFT-1 Nominal Entry - Landing Test Case 1," Informal Memorandum, April 1976.

29. Jones, H.L. and Crawford, B.S., "Space Shuttle Entry and Landing Navigation Analysis," The Analytic Sciences Corp., Technical Report TR-302-2, July 1974.

30. "Orbiter Inertial Measurement Unit (IMU) Azimuth Heading Sensitivity/Thermal Investigation," The Singer Company, Kearfott Division, Document No. Y257A348, January 1977.